



HAL
open science

General formulation of macro-elements for the simulation of multi-layered bonded structures

Sébastien Schwartz, Eric Paroissien, Frederic Lachaud

► **To cite this version:**

Sébastien Schwartz, Eric Paroissien, Frederic Lachaud. General formulation of macro-elements for the simulation of multi-layered bonded structures. *The Journal of Adhesion*, 2020, 96 (6), pp.602-632. 10.1080/00218464.2019.1622420 . hal-02882394

HAL Id: hal-02882394

<https://hal.science/hal-02882394>

Submitted on 26 Jun 2020

HAL is a multi-disciplinary open access archive for the deposit and dissemination of scientific research documents, whether they are published or not. The documents may come from teaching and research institutions in France or abroad, or from public or private research centers.

L'archive ouverte pluridisciplinaire **HAL**, est destinée au dépôt et à la diffusion de documents scientifiques de niveau recherche, publiés ou non, émanant des établissements d'enseignement et de recherche français ou étrangers, des laboratoires publics ou privés.



Open Archive Toulouse Archive Ouverte (OATAO)

OATAO is an open access repository that collects the work of some Toulouse researchers and makes it freely available over the web where possible.

This is an author's version published in: <https://oatao.univ-toulouse.fr/23949>

Official URL : <https://doi.org/10.1080/00218464.2019.1622420>

To cite this version :

Schwartz, Sébastien and Paroissien, Eric and Lachaud, Frédéric General formulation of macro-elements for the simulation of multi-layered bonded structures. (2020) Journal of Adhesion, 96 (6). 602-632. ISSN 0021-8464

Any correspondence concerning this service should be sent to the repository administrator:

tech-oatao@listes-diff.inp-toulouse.fr

General formulation of macro-elements for the simulation of multi-layered bonded structures.

Sébastien Schwartz^{1,2,*}, Eric Paroissien², Frédéric Lachaud²

¹ SOGETI High Tech, R&D Dpt., Aeropark, 3 Chemin de Laporte, 31100 Toulouse, France

² Institut Clément Ader (ICA), Université de Toulouse, ISAE-SUPAERO, INSA, IMT MINES ALBI, UTIII, CNRS, 3 Rue Caroline Aigle, 31400 Toulouse, France

*To whom correspondence should be addressed. E-mail: sebastien.schwartz@sogeti.com

Abstract – Adhesively bonded joints are often addressed through Finite Element (FE). However, analyses based on FE models are computationally expensive, especially when the number of adherends increases. Simplified approaches are suitable for intensive parametric studies. Firstly, a resolution approach for a 1D-beam simplified model of bonded joint stress analysis under linear elastic material is presented. This approach, named the macro-element (ME) technique, is presented and solved through two different methodologies. Secondly, a new methodology for the formulation of ME stiffness matrices is presented. This methodology offers the ability to easily take into account for the modification of simplifying hypotheses while providing the shape of solutions, which reduced then the computational time. It is illustrated with the 1D-beam ME resolution and compared with the previous ones. Perfect agreement is shown. Thirdly, a 1D-beam multi-layered ME formulation involving various local equilibrium equations and constitutive equations is described. It is able to address the stress analysis of multi-layered structures. It is illustrated on a double lap joint (DLJ) with the presented method.

Key words: *macro-element; multi-layered; ordinary differential equation procedure; analytical models; stress analysis; aeronautical.*

NOMENCLATURE AND UNITS

A_j	extensional stiffness (N) of adherend j
B_j	extensional and bending coupling stiffness (N.mm) of the adherend j
D_j	bending stiffness (N.mm ²) of the adherend j
E_a	Young's modulus (MPa) of the adhesive
E_j	Young's modulus (MPa) of the adherend j
G_a	Coulomb's modulus (MPa) of the adhesive
G_j	Coulomb's modulus (MPa) of the adherend j
$k_{i,j}$	peel stiffness (MPa/mm) of the adhesive i
$k_{s,i}$	shear stiffness (MPa/mm) of the adhesive i
k_v	peel stiffness (MPa/mm) of the spring of the adhesive in the SLJ geometry
k_u	shear stiffness (MPa/mm) of the spring of the adhesive in the SLJ geometry
k_{vi}	peel stiffness (MPa/mm) of the spring of the adhesive i in the DLJ geometry
k_{ui}	shear stiffness (MPa/mm) of the spring of the adhesive i in the DLJ geometry
K	stiffness matrix
U	vector of nodal displacements
F	vector of nodal forces
C	vector of integration constants
Y	vector of differential equations solution
S	peel stress (MPa) of the adhesive
S_i	peel stress (MPa) of the adhesive i
T	shear stress (MPa) of the adhesive
T_i	shear stress (MPa) of the adhesive i
V_j	shear force (N) of the adherend j in the y direction
N_j	normal force (N) of the adherend j in the x direction
M_j	bending moment (N.mm) of the adherend j around the z direction

b	width (mm) of the adherends
e_j	thickness (mm) of the adherend j
t_j	thickness (mm) of the adhesive j
l_j	length (mm) of the out-bonded adherend j
L_j	length (mm) of the bonded adherend j
u_j	displacement (mm) of the adherend j in the x direction
v_j	displacement (mm) of the adherend j in the y direction
ϑ_j	angular displacement (rad) of the adherend j around the z direction
$P(x)$	characteristic polynomial
λ_i	eigenvalues i
V_i	eigen vectors i
P	basis change matrix
\oplus	direct sum
J_i	Jordan block i
δ	Kronecker delta
det	determinant of a matrix
dim	dimension of a matrix or vector
ker	kernel of a matrix
Re(x)	real part of x
Im(x)	imaginary part of x
(x,y,z)	system of axes
FE	Finite Element
ME	macro-mlement
ODE	ordinary differential equation
SLJ	single lap joint
DLJ	double lap joint

1. Introduction

In the frame of the design of lightweight structures such as aircraft structures, the proper choice of joining technology is decisive for its life. If the mechanical fastening, including riveting or screwing, is the joining technology the most used on aircraft structures, adhesive bonding may offer significantly improved mechanical performance in terms of stiffness, static strength and fatigue strength [1–4]. For example, according to Higgins, adhesive bonding has been and is used for joining stringers to fuselage and wing skins, in order to stiffen them against buckling [2]. The Finite Element (FE) method is able to address the stress analysis of bonded joints. Nevertheless, since analyses based on FE models are computationally costly, it would be profitable both to restrict them to refined analyses and to develop for designers simplified approaches, enabling extensive parametric studies. Numerous simplified stress analyses of bonded joints are available and provide accurate predictions [5–7]. In 1938, Volkersen published a shear lag model for the prediction of the adhesive shear stress distribution along the overlap [8]. It was the first stress analysis including the deformation of adherends. The adhesive layer was simulated as an elastic foundation of shear springs. In 1944, Goland and Reissner provided the first closed-form solution of distributions of adhesive shear stresses along the overlap for simply supported balanced joint made of adherends undergoing cylindrically bending [9]. The approach used by Goland and Reissner involved two steps: (i) analysis of the bonded overlap leading to integration constants and (ii) analysis of the parts outside the bonded overlap providing the required boundary conditions. This approach is related to the sandwich-type analysis concept for the stress analysis of bonded joints. Goland and Reissner took into account the geometrical non-linearity due to the lag of neutral line to assess the bending moment at both overlap ends, as boundary conditions for the adhesive stress distributions, through a bending moment factor. The sandwich-type analysis concept was then employed by other researchers to improve this initial model to take into different local equilibriums, different constitutive behaviors and various geometries [10–20] eventually leading to various forms of the bending moment factor. Nevertheless, as function of the set of initial simplifying hypotheses, it is not always possible to get closed-form solutions of adhesive

stress distribution. Twenty years ago, Mortensen et al. provided then a resolution scheme based on the numerical integration of first order ordinary differential equations (ODEs) allowing to take account various boundary conditions, geometries and material behaviors [21–23]. The authors of the present papers and co-workers have been working on the development of the macro-element (ME) technique for the simplified stress analysis of bonded, bolted and hybrid (bonded/bolted) joints [24–32]. Dedicated 4-nodes Bonded-bars (BBa) and Bonded-beams (BBe) have been formulated. As for the JE model, only one BBa or BBe, depending on the chosen kinematics, is sufficient to be representative for an entire bonded overlap in the frame of a linear elastic analysis (see Fig. 1). When the geometrical or material properties of the adherends or the adhesive layer vary along the overlap, a mesh is necessary along the overlap length direction only. The ME technique is inspired by the FE method and differs in the sense that the interpolation functions are not assumed. Indeed, they take the shape of solutions of the governing ordinary differential equations (ODEs) system, coming from the constitutive equations of the adhesive and adherends and from the local equilibrium equations, related to the simplifying hypotheses. The main work is thus the formulation of the elementary stiffness matrix of the ME. Once the stiffness matrix of the complete structure is assembled from the elementary matrices and the boundary conditions are applied, the minimization of the potential energy provides the solution, in terms of adhesive stress distributions along the overlap, internal forces and displacements in the adherends. The ME technique can be regarded as mathematical procedure allowing for the resolution of the system of ODE, under a less restricted application field of simplifying hypotheses, in terms of geometry, material behaviors, kinematics, boundary conditions and loadings. In the case of bar kinematics, the closed-form expressions for the stiffness matrix components were provided [24, 27, 28, 32] as well as the shape of adhesive shear stress, adherend displacements and forces. The minimization of the potential energy allows then for the assessment of integration constants. In the case of beam kinematics, if the closed-form expressions for the stiffness matrix components were not provided, those for the adhesive shear and peel stresses, adherend displacements and forces were established after a long work [24, 27, 28]. To speed up the formulation

of new MEs under various sets of hypotheses, another approach has been developed, based on the resolution of the first order ODEs using the exponential matrix. However, the closed-form expressions for adhesive stresses, adherend displacements and forces are not any more provided, so that a meshing along the longitudinal axis is required to assess them along the overlap. If the configuration to be simulated, such as functionally graded or mixed adhesive joints or joints involving non-linear materials, needs a mesh this drawback does not have any consequence in terms of computational time. Nevertheless, in the case homogeneous adhesive joints or joints involving linear material behaviors, the computational time is increased. The objective of this paper is to provide a methodology to formulate new MEs while providing the shape of solutions for the adhesive peel and shear stresses, adherend displacements and internal forces. Firstly, the new method is explained and applied to the original linear elastic 1D-beam model for the stress analysis of a SLJ joint. Secondly, a ME representing for the layering of n adherends is described. Thirdly, the particular case of double lap joint (DLJ) is presented.

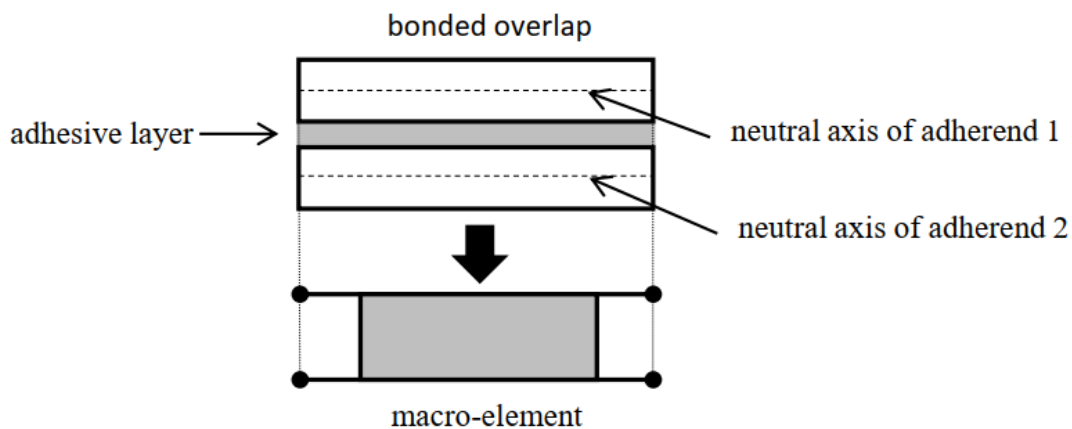


Figure 1. Equivalent modelling of a bonded overlap by a macro-element.

2. Linear Elastic 1D-Beam Model

2.1. Overview

The method presented in this article is applied on the formulation of a ME. A ME is a special finite element developed by Paroissien [24]. It provides the resolution of the bonded overlap system of

governing ODEs. The displacements and forces of both adherends, as well as the adhesive stresses, are then computed. The simplified linear elastic 1D-beam model is a bonded overlap element using four nodes. The outer adherends are Euler-Bernoulli laminated beam. According to the classical Finite Element method, the stiffness matrix of the entire structure K is assembled and the selected boundary conditions are applied. Then, solving the equation $F=KU$, where F is the vector of nodal forces and U is the vector of nodal displacements, leads to the minimization of the potential energy. Using the ME technique offers the possibility to simulate complex structures, such as single-lap bonded joints at low computational costs. The model is based on the following hypotheses:

- the adherends are simulated by linear elastic Euler-Bernoulli laminated straight beams with constant cross-section along the overlap;
- the thickness of the adhesive layer is constant along the overlap;
- the adhesive layer is simulated by an infinite number of linear elastic shear and peel supporting both adherends interfaces, so that the adhesive stress tensor is reduced to the (in-plane) shear stress and peel stress components;
- the adhesive stresses are constant through the adhesive thickness.

This model belongs to the classical sandwich-type models [8–17, 19, 20] for which the adhesive layer is modelled by a bed of shear and peel springs. It suffers then from the same limitations. As a result, the adhesive shear stress does not vanish at both overlap ends. Moreover, this model is unable to predict the actual stress state at the interface between the adherends and the adhesive layer. The stress state predicted by this model tends to be the one along the adhesive neutral line predicted by FE analyses [28, 29]. The adherends are modelled as straight beams. The cases where the adherends are curves are then not supported. Moreover, the cross-section remains constant along the overlap. To take into account a variation of geometrical and/or material properties of adherends and/or adhesive, an approach could be to mesh the joint by MEs with homogeneous properties; these properties vary along the overlap, as it was done for the case of functionally graded adhesive joints [32]. The Euler-Bernoulli kinematics is not a restriction. The ME could be formulated with a

Timoshenko beam model [32]. Moreover, for thin adherends, both beam models leads to similar linear elastic predictions [29]. The analysis is geometrically linear. The second order effect on strains is not taken into account, while the equilibrium is not updated. It is indicated that an approximation of the geometrical nonlinear, without involving an iterative analysis procedure, is presented in [32]; it is based on the local equilibrium of adherends by Luo and Tong [19] which allows a coupling between the bending moment and the normal forces. Besides, in order to take into account the secondary bending moment on the adhesive stress distributions, it is common to load the sandwich edges with relevant forces, moments or displacement analytically or numerically computed [14, 17, 24]. Finally, as related to the 1D kinematics, only in-plane loadings can be considered.

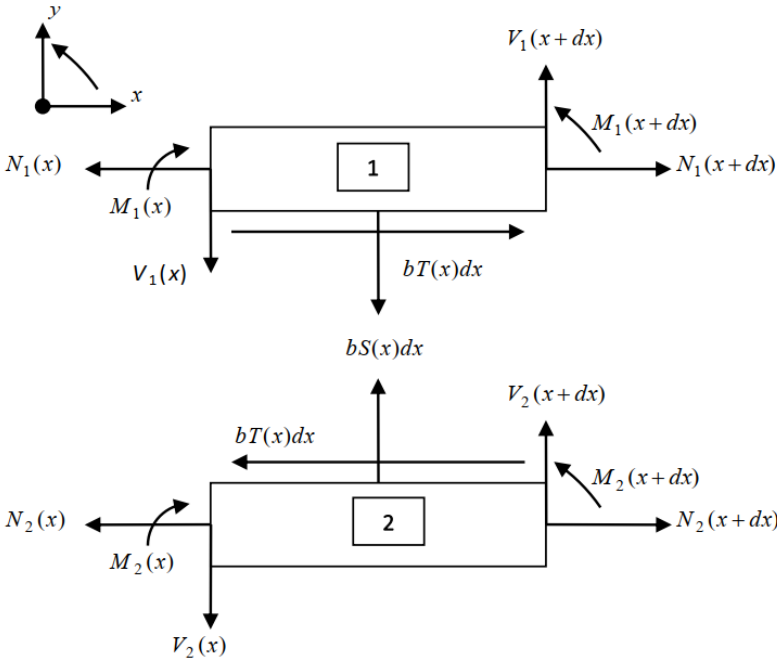


Figure 2. Free body diagram of two bonded adherends under 1D-beam kinematics.

2.2. Governing equations

The local equilibrium of an isolated portion dx of both adherends (Fig. 2) provides the following set of six equations:

$$\begin{cases} \frac{dN_j}{dx} = (-1)^j bT \\ \frac{dV_j}{dx} = (-1)^{j+1} bS \\ \frac{dM_j}{dx} + V_j + \frac{e_j}{2} bT = 0 \end{cases} \quad \text{with } j = 1,2 \quad (1)$$

where S and T are respectively the adhesive peel and shear stress, N_j and V_j are respectively the normal and shearing force in adherend j , M_j are the bending moment in adherend j , b is the width and e_j is the thickness of the adherend j . Note that Eq. (1) refers to the local equilibrium derived and employed by [9]. The adhesive is considered linear elastic and as raised previously, simulated by an infinite number of elastic shear and peel springs. The adhesive spring relationships are such as:

$$\begin{cases} T = \frac{G_a}{e} \left(u_2 - u_1 - \frac{e_1}{2} \theta_1 - \frac{e_2}{2} \theta_2 \right) \\ S = \frac{E_a}{e} (v_1 - v_2) \end{cases} \quad (2)$$

where E_a , G_a are respectively the peel and shear modulus of the adhesive, e is the adhesive thickness, u_j , v_j , θ_j are respectively the longitudinal displacement, the deflection and the bending angle of the adherend j .

$$\begin{cases} N_j = A_j \frac{du_j}{dx} - B_j \frac{d^2v_j}{dx^2} \\ M_j = -B_j \frac{du_j}{dx} + D_j \frac{d^2v_j}{dx^2} \\ \theta_j = \frac{dv_j}{dx} \end{cases} \quad \text{with } j = 1,2 \quad (3)$$

where A_j is the extensional stiffness, B_j the coupling stiffness, D_j the bending stiffness. Further details on these constitutive equations can be found in standard textbooks on composite mechanics [33, 34].

For isotropic materials, the stiffnesses are found under the following shape:

$$\begin{cases} A_j = bE_j e_j \\ B_j = 0 \\ D_j = \frac{bE_j e_j^3}{12} \end{cases} \quad \text{with } j = 1,2 \quad (4)$$

2.3. Stiffness matrix

Eq. (2) can be expressed as:

$$\begin{cases} \frac{du_j}{dx} = \frac{D_j N_j + B_j M_j}{\Delta_j} \\ \frac{d^2 v_j}{dx^2} = \frac{A_j M_j + B_j N_j}{\Delta_j} \end{cases} \quad \text{with } j = 1, 2 \quad (5)$$

where $\Delta_j = A_j D_j - B_j^2$ is assumed to be not equal to zero. By combining Eqs. (1), (2), (3), and (5), the following differential equation system in terms of adhesive stresses is obtained:

$$\begin{cases} \frac{d^3 T}{dx^3} = k_1 \frac{dT}{dx} + k_2 S \\ \frac{d^4 S}{dx^4} = -k_3 \frac{dT}{dx} - k_4 S \end{cases} \quad (6)$$

where:

$$\begin{cases} k_1 = \frac{G_{ab}}{e} \left[\frac{D_1}{\Delta_1} \left(1 + \frac{A_1 e_1 (e_1 + e)}{4D_1} \right) + \frac{D_2}{\Delta_2} \left(1 + \frac{A_2 e_2 (e_2 + e)}{4D_2} \right) + \left(\frac{B_1}{\Delta_1} \left(e_1 + \frac{e}{2} \right) - \frac{B_2}{\Delta_2} \left(e_2 + \frac{e}{2} \right) \right) \right] \\ k_2 = \frac{G_{ab}}{e} \left[\frac{e_1 A_1}{2\Delta_1} - \frac{e_2 A_2}{2\Delta_2} + \left(\frac{B_1}{\Delta_1} + \frac{B_2}{\Delta_2} \right) \right] \\ k_3 = \frac{E_{ab}}{e} \left[\frac{(e_1 + e) A_1}{2\Delta_1} - \frac{(e_2 + e) A_2}{2\Delta_2} + \left(\frac{B_1}{\Delta_1} + \frac{B_2}{\Delta_2} \right) \right] \\ k_4 = \frac{E_{ab}}{e} \left[\frac{A_1}{\Delta_1} + \frac{A_2}{\Delta_2} \right] \end{cases} \quad (7)$$

By successive differentiations and linear combinations, the system Eq. (6) can be uncoupled as:

$$\begin{cases} \frac{d^6 S}{dx^6} - k_1 \frac{d^4 S}{dx^4} + k_4 \frac{d^2 S}{dx^2} + S(k_2 k_3 - k_1 k_4) = 0 \\ \frac{d}{dx} \left(\frac{d^6 T}{dx^6} - k_1 \frac{d^4 T}{dx^4} + k_4 \frac{d^2 T}{dx^2} + T(k_2 k_3 - k_1 k_4) \right) = 0 \end{cases} \quad (8)$$

The resolution of the system Eq. (8) leads to the determination of the nodal displacements and forces as functions of the adhesive stresses and their derivatives. The nodal displacements and forces are the key parameters for the determination of the ME stiffness matrix. Their computation for each adherend is fully detailed in [27, 28]. It is shown that the problem depends of 12 integration constants named c_i with $i \in [1, 12]$ written under the following vector form:

$$\mathcal{C} = [c_1 \quad c_2 \quad c_3 \quad c_4 \quad c_5 \quad c_6 \quad c_7 \quad c_8 \quad c_9 \quad c_{10} \quad c_{11} \quad c_{12}]^T \quad (9)$$

The superscript ' T ' indicates the transposition. The nodal displacements and forces are computed from their values at $x = 0$ and $x = \Delta$ as:

$$U = \begin{pmatrix} u_i \\ u_j \\ u_k \\ u_l \\ v_i \\ v_j \\ v_k \\ v_l \\ \theta_i \\ \theta_j \\ \theta_k \\ \theta_l \end{pmatrix} = \begin{pmatrix} u_1(0) \\ u_2(0) \\ u_1(\Delta) \\ u_2(\Delta) \\ v_1(0) \\ v_2(0) \\ v_1(\Delta) \\ v_2(\Delta) \\ \theta_1(0) \\ \theta_2(0) \\ \theta_1(\Delta) \\ \theta_2(\Delta) \end{pmatrix} = MC \quad \text{and} \quad F = \begin{pmatrix} Q_i \\ Q_j \\ Q_k \\ Q_l \\ R_i \\ R_j \\ R_k \\ R_l \\ S_i \\ S_j \\ S_k \\ S_l \end{pmatrix} = \begin{pmatrix} -N_1(0) \\ -N_2(0) \\ N_1(\Delta) \\ N_2(\Delta) \\ -V_1(0) \\ -V_2(0) \\ V_1(\Delta) \\ V_2(\Delta) \\ -M_1(0) \\ -M_2(0) \\ M_1(\Delta) \\ M_2(\Delta) \end{pmatrix} = NC \quad (10)$$

where Q , R and S respectively refer to the nodal normal forces, shear forces and bending moments. It is shown that M and N matrix are linearly dependent on the same 12 integration constants listed in Eq. (9). The ME stiffness matrix can be computed as:

$$K = N \cdot M^{-1} \quad (11)$$

2.4. Methods of resolution

The system Eq. (8) can be solved in different ways to obtain the expressions for the nodal displacements and forces. A first way consists in using the differential equation theory (see Appendix A1). This method of resolution is useful but it is a heavy process and relies on the ability to uncouple the final system of equations to get a solution. Another way involves the matrix properties. The matrix representation is a powerful way for managing complex differential equation systems. Resolutions from the theory of differential equations can be used with matrix theories. By combining Eqs. (2), (3), and (4), the system in Eq. (1) becomes:

$$\begin{aligned} \frac{d^2 u_1}{dx^2} &= \left(\frac{G_a b}{eA_1}\right) u_1 + \left(-\frac{G_a b}{eA_1}\right) u_2 + \left(\frac{G_a b e_1}{2eA_1}\right) \frac{dv_1}{dx} + \left(\frac{G_a b e_2}{2eA_1}\right) \frac{dv_2}{dx} \\ \frac{d^2 u_2}{dx^2} &= \left(-\frac{G_a b}{eA_2}\right) u_1 + \left(\frac{G_a b}{eA_2}\right) u_2 + \left(-\frac{G_a b e_1}{2eA_2}\right) \frac{dv_1}{dx} + \left(-\frac{G_a b e_2}{2eA_2}\right) \frac{dv_2}{dx} \\ \frac{d^4 v_1}{dx^4} &= \left(-\frac{E_a b}{eD_1}\right) v_1 + \left(\frac{E_a b}{eD_1}\right) v_2 + \left(\frac{G_a b e_1}{2eD_1}\right) \frac{du_1}{dx} + \left(-\frac{G_a b e_1}{2eD_1}\right) \frac{du_2}{dx} + \left(\frac{G_a b e_1^2}{4eD_1}\right) \frac{d^2 v_1}{dx^2} + \left(\frac{G_a b e_1 e_2}{4eD_1}\right) \frac{d^2 v_2}{dx^2} \\ \frac{d^4 v_2}{dx^4} &= \left(\frac{E_a b}{eD_2}\right) v_1 + \left(-\frac{E_a b}{eD_2}\right) v_2 + \left(\frac{G_a b e_2}{2eD_2}\right) \frac{du_1}{dx} + \left(-\frac{G_a b e_2}{2eD_2}\right) \frac{du_2}{dx} + \left(\frac{G_a b e_1 e_2}{4eD_2}\right) \frac{d^2 v_1}{dx^2} + \left(\frac{G_a b e_2^2}{4eD_2}\right) \frac{d^2 v_2}{dx^2} \end{aligned} \quad (12)$$

Supposing a Y vector and its derivate as:

$$Y = \left[u_1 \quad u_2 \quad v_1 \quad v_2 \quad \frac{du_1}{dx} \quad \frac{du_2}{dx} \quad \frac{dv_1}{dx} \quad \frac{dv_2}{dx} \quad \frac{d^2v_1}{dx^2} \quad \frac{d^2v_2}{dx^2} \quad \frac{d^3v_1}{dx^3} \quad \frac{d^3v_2}{dx^3} \right]^T \quad (13)$$

$$\frac{dY}{dx} = \left[\frac{du_1}{dx} \quad \frac{du_2}{dx} \quad \frac{dv_1}{dx} \quad \frac{dv_2}{dx} \quad \frac{d^2u_1}{dx^2} \quad \frac{d^2u_2}{dx^2} \quad \frac{d^2v_1}{dx^2} \quad \frac{d^2v_2}{dx^2} \quad \frac{d^3v_1}{dx^3} \quad \frac{d^3v_2}{dx^3} \quad \frac{d^4v_1}{dx^4} \quad \frac{d^4v_2}{dx^4} \right]^T \quad (14)$$

the set of equations in Eq. (12) can be rewritten under the matrix form as:

$$\frac{dY}{dx} = A.Y \quad (15)$$

with A , a square matrix provided in Appendix A2.

A well-known solution of a differential equation with constant coefficients such as Eq. (24) is:

$$Y(x) = e^{A.x}C \quad (16)$$

where C is the integration constant (see Eq. (9)).

The power series gives the exponential of a real or complex square matrix M such as:

$$e^M = \sum_{k \in \mathbb{N}} \frac{1}{k!} M^k \quad (17)$$

Most software use a predefined threshold of convergence to determine the exponential of a matrix as a numerical approximation. Doing so, Eqs. (16) and (17) lead to the numerical nodal displacements and forces to compute Eq. (10) which provides the stiffness matrix with Eq. (11). The inconvenient with this method is the numerical approximation aspect. Because of the exponential estimation, it is impossible to get the exact analytical solution. Therefore, a new method is needed.

3. New method for the ME formulation

3.1. Formulation

The aforementioned method wants to explain the analytical solution of a matrix system of differential equations. Taking into consideration the system Eq. (15), the matrix A is a squared matrix $n \times n$, with $n = 12$. It exists an invertible matrix P such as $J = P^{-1}.A.P$ where J is the Jordan normal form [35–40]. According to [41–43], it corresponds to a generalization of the diagonalization procedure where a diagonalizable matrix is a particular case. Thus, any squared matrix has a Jordan normal form [44]. Therefore, Eq. (15) becomes:

$$\frac{dZ}{dx} = J.Z \quad \text{with} \quad Z = P^{-1}.Y \quad (18)$$

which is a differential equation matrix system with constant coefficients. Using the same reasoning as Eq. (15), the shape of the solution of differential equation with constant coefficient Eq. (18) is:

$$Z = e^{J.x}C \quad (19)$$

By combining with Eq. (18), the final solution is:

$$Y = P.e^{J.x}.C \quad (20)$$

3.2. Generation of solution

The exponential part corresponds to the term $e^{J.x}$ of Eq. (20). To determinate the J matrix, the Jordan method (or Jordan normal form) is used. This method relies on eigenvalues and eigenvectors research problem. The relation Eq. (21), leads to the characteristic polynomial of A where I is the $n \times n$ identity matrix and λ are eigenvalues of A .

$$P(\lambda) = \det(\lambda.I - A) \quad (21)$$

Using Eq. (77) with Eq. (21) it provides the same characteristic polynomial expression as Eq. (68). The geometric multiplicity (m_{geo}) [57] of each eigenvalue λ_i gives the number of Jordan blocks thanks to the dimension (written "dim") of the kernel (written "ker") of the transformation $(A - \lambda_i.I)$ such as:

$$m_{geo} = \dim \ker(A - \lambda_i.I) \quad (22)$$

Appling Eq. (22) to Eq. (68) knowing λ_i with $i = 1...7$, the geometric multiplicities are summarized in the Table 2.

Table 2. Geometric multiplicity (or number of Jordan block) for each eigenvalue of A .

Eigenvalues	Geometric multiplicity
$\lambda_1, \lambda_2, \lambda_3, \lambda_4, \lambda_5, \lambda_6$	1
λ_7	2

The following formula gives the number of Jordan blocks of size j [45]:

$$2 \dim \ker(A - \lambda_i \cdot I)^j - \dim \ker(A - \lambda_i \cdot I)^{j+1} - \dim \ker(A - \lambda_i \cdot I)^{j-1} \quad (23)$$

Using the relation Eq. (23), the number of Jordan blocks are summarize as:

- one block of size four and one block of size two for $P_1(\lambda)$ eigenvalues
- each $P_2(\lambda)$ eigenvalues have one block of size one

Then, the general form of the matrix J is provided such as:

$$J = \bigoplus_i J_j(\lambda_i) \quad (24)$$

where \bigoplus is the direct sum and J is a squared matrix, called the Jordan normal form of A for a given eigenvalue λ_i , with the form:

$$J_i = \begin{bmatrix} \lambda_i & 1 & 0 & 0 \\ 0 & \lambda_i & \ddots & 0 \\ \vdots & \ddots & \ddots & 1 \\ 0 & \dots & 0 & \lambda_i \end{bmatrix} \quad (25)$$

The combination of Eq. (24) with Eq. (25) gives:

$$J = J_1(\lambda_1) \oplus J_1(\lambda_2) \oplus J_1(\lambda_3) \oplus J_1(\lambda_4) \oplus J_1(\lambda_5) \oplus J_1(\lambda_6) \oplus J_4(\lambda_7) \oplus J_2(\lambda_7) \quad (26)$$

The matrix J is similar to a block diagonal matrix as:

$$J = \begin{bmatrix} J_1(\lambda_1) & 0 & 0 & 0 & 0 & 0 & 0 & 0 \\ 0 & J_1(\lambda_2) & 0 & 0 & 0 & 0 & 0 & 0 \\ 0 & 0 & J_1(\lambda_3) & 0 & 0 & 0 & 0 & 0 \\ 0 & 0 & 0 & J_1(\lambda_4) & 0 & 0 & 0 & 0 \\ 0 & 0 & 0 & 0 & J_1(\lambda_5) & 0 & 0 & 0 \\ 0 & 0 & 0 & 0 & 0 & J_1(\lambda_6) & 0 & 0 \\ 0 & 0 & 0 & 0 & 0 & 0 & J_4(\lambda_7) & 0 \\ 0 & 0 & 0 & 0 & 0 & 0 & 0 & J_2(\lambda_7) \end{bmatrix} \quad (27)$$

The exponential part of Eq. (20) becomes:

$$e^{J \cdot x} = \begin{bmatrix} e^{J_1(\lambda_1) \cdot x} & 0 & 0 & 0 & 0 & 0 & 0 & 0 \\ 0 & e^{J_1(\lambda_2) \cdot x} & 0 & 0 & 0 & 0 & 0 & 0 \\ 0 & 0 & e^{J_1(\lambda_3) \cdot x} & 0 & 0 & 0 & 0 & 0 \\ 0 & 0 & 0 & e^{J_1(\lambda_4) \cdot x} & 0 & 0 & 0 & 0 \\ 0 & 0 & 0 & 0 & e^{J_1(\lambda_5) \cdot x} & 0 & 0 & 0 \\ 0 & 0 & 0 & 0 & 0 & e^{J_1(\lambda_6) \cdot x} & 0 & 0 \\ 0 & 0 & 0 & 0 & 0 & 0 & e^{J_4(\lambda_7) \cdot x} & 0 \\ 0 & 0 & 0 & 0 & 0 & 0 & 0 & e^{J_2(\lambda_7) \cdot x} \end{bmatrix} \quad (28)$$

As explained previously, the Jordan blocks J_i corresponding to λ_i respectively take the shape $\lambda_i \cdot I + N$ where N (nilpotent matrix) is defined such as $N_{i,j} = \delta_{i,j+1}$ (δ is the Kronecker delta) and I is the

identity matrix. This form is the Jordan-Chevalley decomposition [46, 47]. Using the nilpotent matrix properties and Eq. (17), Eq. (28) becomes:

$$e^{J.x} = \begin{bmatrix} e^{\lambda_1.x} & 0 & 0 & 0 & 0 & 0 & 0 & 0 & 0 & 0 & 0 & 0 \\ 0 & e^{\lambda_2.x} & 0 & 0 & 0 & 0 & 0 & 0 & 0 & 0 & 0 & 0 \\ 0 & 0 & e^{\lambda_3.x} & 0 & 0 & 0 & 0 & 0 & 0 & 0 & 0 & 0 \\ 0 & 0 & 0 & e^{\lambda_4.x} & 0 & 0 & 0 & 0 & 0 & 0 & 0 & 0 \\ 0 & 0 & 0 & 0 & e^{\lambda_5.x} & 0 & 0 & 0 & 0 & 0 & 0 & 0 \\ 0 & 0 & 0 & 0 & 0 & e^{\lambda_6.x} & 0 & 0 & 0 & 0 & 0 & 0 \\ 0 & 0 & 0 & 0 & 0 & 0 & 1 & x & \frac{x^2}{2} & \frac{x^3}{6} & 0 & 0 \\ 0 & 0 & 0 & 0 & 0 & 0 & 0 & 1 & x & \frac{x^2}{2} & 0 & 0 \\ 0 & 0 & 0 & 0 & 0 & 0 & 0 & 0 & 1 & x & 0 & 0 \\ 0 & 0 & 0 & 0 & 0 & 0 & 0 & 0 & 0 & 1 & 0 & 0 \\ 0 & 0 & 0 & 0 & 0 & 0 & 0 & 0 & 0 & 0 & 1 & x \\ 0 & 0 & 0 & 0 & 0 & 0 & 0 & 0 & 0 & 0 & 0 & 1 \end{bmatrix} \quad (29)$$

The resolution of the eigenvector problem Eq. (30) for each $P_1(\lambda)$ eigenvalues leads to the set Eq. (31).

$$A.v_i = \lambda_i.v_i \quad (30)$$

$$V_1 = \{v_1, v_2, v_3, v_4, v_5, v_6\} \quad (31)$$

Jordan chains provide the eigenvectors set of each Jordan block [48]. The generalized eigenvector relation is:

$$x_j = (A - \lambda.I)^{m-j}.x_m \quad \text{with} \quad x_m \in \ker(A - \lambda.I)^m \quad (32)$$

where m is the Jordan block size and j is the vector index. Using the relation Eq. (32), the eigenvector of a Jordan block of size four and two are respectively:

$$V_2 = \{A^3.x_4, A^2.x_4, A.x_4, x_4\} \quad \text{with} \quad x_4 \in \ker A^4 \quad (33)$$

$$V_3 = \{A.x_2, x_2\} \quad \text{with} \quad x_2 \in \ker A^2 \quad (34)$$

The concatenation of those three vector sets leads to the P invertible matrix building as:

$$P = [V_1, V_2, V_3] \quad (35)$$

A transformation from the complex space \mathbb{C} to real space \mathbb{R} manages complex eigenvalues and eigenvectors. The transformation is applied for two conjugate complex numbers named respectively λ_k and $\overline{\lambda_k}$. For each line j of an eigenvector q_k (respectively $q_{k+1} = \overline{q_k}$) linked to an eigenvalue λ_k (respectively $\lambda_{k+1} = \overline{\lambda_k}$):

$$\begin{cases} f_k(x) = q_{j,k} e^{\lambda_k x} = (q_{j,k}^0 + i \cdot q_{j,k}^*) e^{\lambda_k^0 \cdot x} [\cos(\lambda_k^* \cdot x) + i \cdot \sin(\lambda_k^* \cdot x)] \\ f_{k+1}(x) = \overline{q_{j,k}} e^{\lambda_k x} = (q_{j,k}^0 - i \cdot q_{j,k}^*) e^{\lambda_k^0 \cdot x} [\cos(\lambda_k^* \cdot x) - i \cdot \sin(\lambda_k^* \cdot x)] \end{cases} \quad (36)$$

where:

- λ_k^0 and $q_{j,k}^0$ are respectively the real part of λ_k and $q_{k,j}$
- λ_k^* and $q_{j,k}^*$ are respectively the imaginary part of λ_k and $q_{k,j}$

The transformation gives:

$$\begin{cases} g_k(x) = \frac{1}{2}(f_k(x) + f_{k+1}(x)) = Re(f_k(x)) = Re(f_{k+1}(x)) \\ g_{k+1}(x) = \frac{1}{2}(f_k(x) - f_{k+1}(x)) = Im(f_k(x)) = -Im(f_{k+1}(x)) \end{cases} \quad (37)$$

Using Eq. (37) and Eq. (74) in Eq. (29) leads to the following final expression:

$$e^{J \cdot x} = \begin{bmatrix} e^{r \cdot x} & 0 & 0 & 0 & 0 & 0 & 0 & 0 & 0 & 0 & 0 & 0 & 0 \\ 0 & e^{-r \cdot x} & 0 & 0 & 0 & 0 & 0 & 0 & 0 & 0 & 0 & 0 & 0 \\ 0 & 0 & e^{s \cdot x} \cos(t \cdot x) & e^{s \cdot x} \sin(t \cdot x) & 0 & 0 & 0 & 0 & 0 & 0 & 0 & 0 & 0 \\ 0 & 0 & -e^{s \cdot x} \sin(t \cdot x) & e^{s \cdot x} \cos(t \cdot x) & 0 & 0 & 0 & 0 & 0 & 0 & 0 & 0 & 0 \\ 0 & 0 & 0 & 0 & e^{-s \cdot x} \cos(t \cdot x) & e^{-s \cdot x} \sin(t \cdot x) & 0 & 0 & 0 & 0 & 0 & 0 & 0 \\ 0 & 0 & 0 & 0 & -e^{-s \cdot x} \sin(t \cdot x) & e^{-s \cdot x} \cos(t \cdot x) & 0 & 0 & 0 & 0 & 0 & 0 & 0 \\ 0 & 0 & 0 & 0 & 0 & 0 & 1 & x & \frac{x^2}{2} & \frac{x^3}{6} & 0 & 0 & 0 \\ 0 & 0 & 0 & 0 & 0 & 0 & 0 & 1 & x & \frac{x^2}{2} & 0 & 0 & 0 \\ 0 & 0 & 0 & 0 & 0 & 0 & 0 & 0 & 1 & x & 0 & 0 & 0 \\ 0 & 0 & 0 & 0 & 0 & 0 & 0 & 0 & 0 & 0 & 1 & 0 & 0 \\ 0 & 0 & 0 & 0 & 0 & 0 & 0 & 0 & 0 & 0 & 0 & 1 & x \\ 0 & 0 & 0 & 0 & 0 & 0 & 0 & 0 & 0 & 0 & 0 & 0 & 1 \end{bmatrix} \quad (38)$$

Relations Eq. (77) and Eq. (30) leads to the following general eigenvector expression:

$$v_k(\lambda_k) = \begin{bmatrix} 1 \\ v_{21} \\ v_{31} + v_{34}v_{41} \\ v_{41} \\ \lambda_k \\ \lambda_k v_{21} \\ \lambda_k(v_{31} + v_{34}v_{41}) \\ \lambda_k v_{41} \\ \lambda_k^2(v_{31} + v_{34}v_{41}) \\ \lambda_k^2 v_{41} \\ \lambda_k^3(v_{31} + v_{34}v_{41}) \\ \lambda_k^3 v_{41} \end{bmatrix} \quad (39)$$

where:

$$\begin{cases} v_{21} = \left(-\frac{A_1}{A_2} \right) \\ v_{31} = \left(\frac{2eA_1}{G_a b e_1} \lambda_k - \frac{2}{e_1 \lambda_k} - \frac{2A_1}{e_1 A_2 \lambda_k} \right) \\ v_{34} = \left(-\frac{e_2}{e_1} \right) v_{34} v_4 \\ v_{41} = \frac{\frac{E_a b}{e D_1} v_{31} - \frac{G_a b e_1}{2 e D_1} \lambda_k (1 - v_{21}) - \frac{G_a b e_1^2}{4 e D_1} \lambda_k^2 v_{31} + \lambda_k^4 v_{31}}{\frac{E_a b}{e D_1} (1 - v_{34}) + \frac{G_a b e_1}{4 e D_1} \lambda_k^2 (e_2 + e_1 v_{34}) - \lambda_k^4 v_{34}} \end{cases} \quad (40)$$

and v_k is the eigenvector linked to the eigenvalue λ_k . Substituting eigenvalue calculated previously and by using Eq. (37), the last set of vector V_1 is expressed as:

$$V_1 = \{v_1(R_1), v_2(R_2), Re(v_3(R_3)), Im(v_3(R_3)), Re(v_5(R_5)), Im(v_5(R_5))\} \quad (41)$$

The relationships in Eq. (39) and Eq. (41) finally provide the final P matrix by concatenation as:

$$P = [V_1, V_2, V_3] \quad (42)$$

The solution generated by this method is used to build the K stiffness matrix. Finally, using Eqs. (20), (38), and (42), the nodal displacements and forces are then obtained with Eq. (10) leading to the stiffness matrix with Eq. (11).

3.3. Results

The final matrix computed with the aforementioned method was compared to the one provided by [27, 28]. Each stiffness matrix component computed with this new method are strictly the same as those computed with the earlier method [27, 28]. As a result, the use of the ME formulated with the new method of resolution leads to the same predictions as with the use of the earlier formulation. The accuracy of the ME model by itself has already been extensively assessed on the case of the Single Lap Joint in previous published papers [27–30, 49, 50]. Thus, more validations on the linear elastic SLJ case is not necessary. Therefore, in the next section, the linear elastic DLJ case will be explored with the presented approach. With this method, it is easier to address solution of ME governing equations and to keep flexibility on the initial formulation by always using the same resolution technique. The generation of new ME is then more straightforward.

4. Multi-layered macro-element

In this section, a formulation of a multi-layered ME is described. This generalized formulation cover particular cases of SLJ and DLJ. Firstly, the whole formulation is described. Secondly, a particular case, corresponding to DLJ, is studied.

4.1. Formulation

The basis for the formulation is the same than in the previous section. As a result, the hypotheses and associated limitations are the same as described in section 2.1. However, there is an additional one: a linear shear stress variation in the adherend thickness following [16]. This hypothesis will be named TOM. The ME is made of a total of P adherends (or layers). A total number of $P - 1$ adhesive layers (or interfaces) are then involved. Two types of equilibrium are considered at the same time for the ME formulation. The first one named GR type from [9] and the second named HS type from [10–12]. The HS type takes into consideration the adhesive thickness in the local equilibrium bending equation contrary to the GR type. To deal with these two cases, the following function is introduced:

$$h_{i,j}^p = h_i + ph_j' \quad (43)$$

where p is the switching condition:

- If $p = 0$, then the equilibrium is under GR type
- If $p = 1$, then the equilibrium is under HS type

and where h_i is the half-thickness of the adherend i such as $h_i = \frac{e_i}{2}$ and h_j' of the half-thickness of the adhesive j such as $h_j' = \frac{t_j}{2}$ where e_i and t_j are respectively the thickness of the adherend and the adhesive. The local equilibrium of an isolated portion dx of a multi-layered element (Fig. 3) provides the following set of equations:

$$\begin{cases} \frac{dN_1}{dx} + T_1 b = 0 \\ \frac{dV_1}{dx} - S_1 \cdot b = 0 \\ \frac{dM_1}{dx} + V_1 + T_1 b h_{1,1}^p = 0 \end{cases} \quad (44)$$

$$\begin{cases} \frac{dN_i}{dx} - (T_{i-1} - T_i)b = 0 \\ \frac{dV_i}{dx} + (S_{i-1} - S_i) \cdot b = 0 \\ \frac{dM_i}{dx} + V_i + (T_{i-1}h_{i,i-1}^p + T_i h_{i,i}^p)b = 0 \end{cases} \quad \text{with } 2 \leq i \leq P - 1 \quad (45)$$

$$\begin{cases} \frac{dN_P}{dx} - T_{P-1}b = 0 \\ \frac{dV_P}{dx} + S_{P-1} \cdot b = 0 \\ \frac{dM_P}{dx} + V_P + T_{P-1}bh_{P,P-1}^p = 0 \end{cases} \quad (46)$$

The adhesive is considered linear elastic and as raised previously, simulated by an infinite number of elastic shear and peel springs. The adhesive spring relations are:

$$\begin{cases} S_i = k_{I,i}[v_i - v_{i+1}] \\ T_i = k_{II,i}[u_{i+1} - u_i - h_{i+1}\theta_{i+1} - h_i\theta_i] \end{cases} \quad (47)$$

with $1 \leq i \leq P-1$, where $k_{I,i}$ and $k_{II,i}$ are respectively the peel and shear rigidity and h_i the half-thickness of the layer i . For an adherend i , u_i is the longitudinal displacement, v_i the transversal displacement and ϑ_i the bending angle.

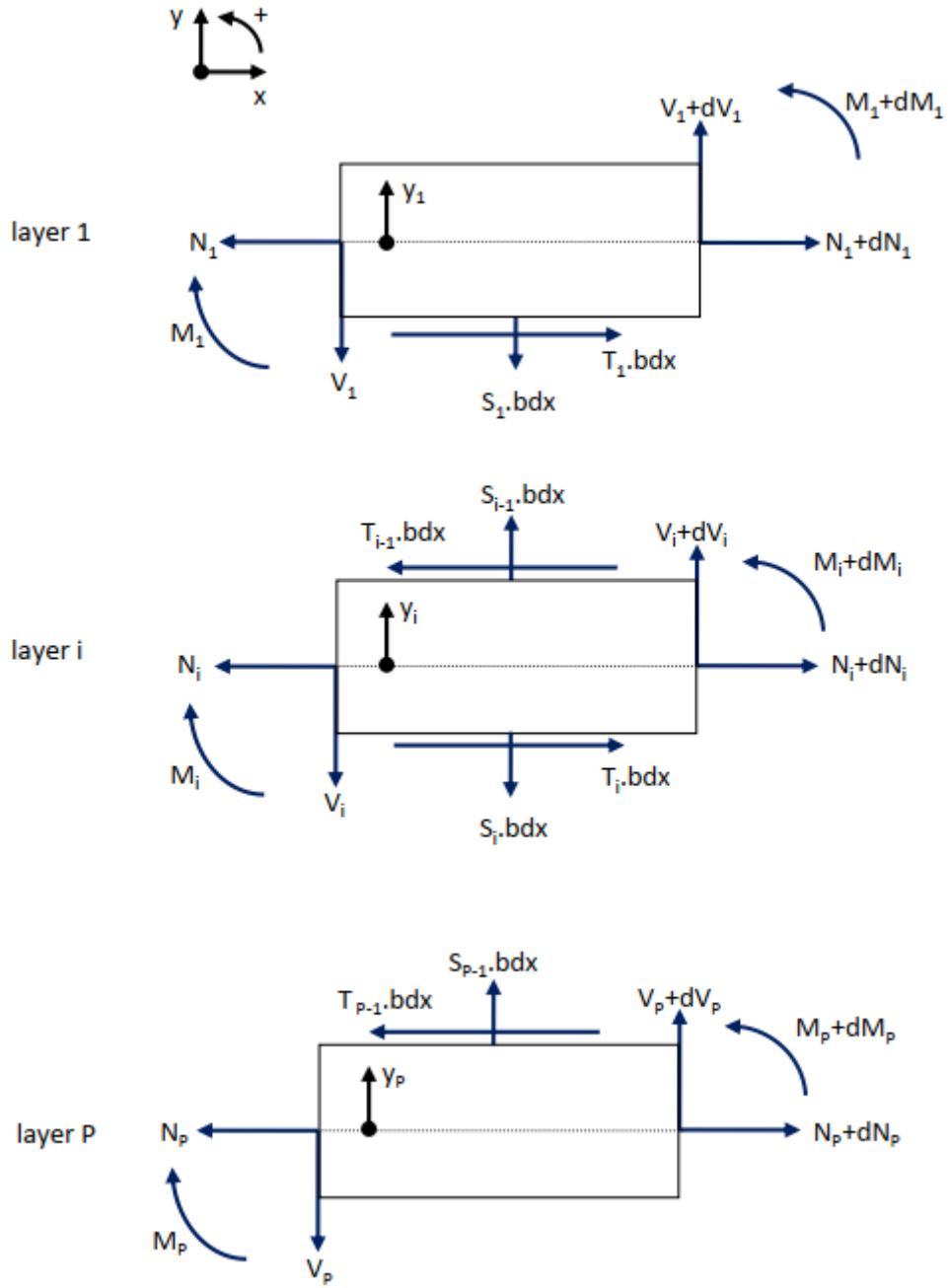


Figure 3. Free body diagram of the 1st, ith and Pth adherends under 1D-beam kinematics.

The constitutive equations considering a shear stress variation in the thickness are [27, 28]:

$$\begin{cases} N_1 = A_1 \frac{du_1}{dx} - B_1 \frac{d\theta_1}{dx} - H_1 \frac{dT_1}{dx} \\ M_1 = -B_1 \frac{du_1}{dx} + D_1 \frac{d\theta_1}{dx} + K_1 \frac{dT_1}{dx} \\ \theta_1 = \frac{dv_1}{dx} \end{cases} \quad (48)$$

$$\begin{cases} N_i = A_i \frac{du_i}{dx} - B_i \frac{d\theta_i}{dx} - H_i \frac{dT_{i-1}}{dx} - H'_i \frac{dT_i}{dx} \\ M_i = -B_i \frac{du_i}{dx} + D_i \frac{d\theta_i}{dx} + K_i \frac{dT_{i-1}}{dx} + K'_i \frac{dT_i}{dx} \\ \theta_i = \frac{dv_i}{dx} \end{cases} \quad \text{with } 2 \leq i \leq P-1 \quad (49)$$

$$\begin{cases} N_P = A_P \frac{du_P}{dx} - B_P \frac{d\theta_P}{dx} - H_P \frac{dT_{P-1}}{dx} \\ M_P = -B_P \frac{du_P}{dx} + D_P \frac{d\theta_P}{dx} + K_P \frac{dT_{P-1}}{dx} \\ \theta_P = \frac{dv_P}{dx} \end{cases} \quad (50)$$

where, for $1 \leq i \leq P$:

$$\begin{cases} H_i = \frac{1}{2G_i} \left(B_i - \frac{1}{2h_i} D_i \right) \\ H'_i = \frac{1}{2G_i} \left(B_i + \frac{1}{2h_i} D_i \right) \end{cases} \quad (51)$$

$$\begin{cases} K_i = \frac{1}{2G_i} \left(D_i - \frac{1}{2h_i} F_i \right) \\ K'_i = \frac{1}{2G_i} \left(D_i + \frac{1}{2h_i} F_i \right) \end{cases} \quad (52)$$

$$\begin{cases} A_i = b \sum_{p_i=1}^{n_i} Q_i^{p_i} \left(h_{p_i} - h_{p_i-1} \right) \\ B_i = \frac{b}{2} \sum_{p_i=1}^{n_i} Q_i^{p_i} \left(h_{p_i}^2 - h_{p_i-1}^2 \right) \\ D_i = \frac{b}{3} \sum_{p_i=1}^{n_i} Q_i^{p_i} \left(h_{p_i}^3 - h_{p_i-1}^3 \right) \\ F_i = \frac{b}{4} \sum_{p_i=1}^{n_i} Q_i^{p_i} \left(h_{p_i}^4 - h_{p_i-1}^4 \right) \end{cases} \quad (53)$$

where A_i is the membrane stiffness, B_i is the coupling membrane-bending stiffness, D_i is the bending stiffness, G_i is the Coulomb's modulus, and $Q_i^{p_i}$ is the matrix of reduced stiffness in the p_i^{th} ply of the adherend i . As in the previous section, the system can be written as:

$$\frac{dY}{dx} = A.Y \quad (54)$$

with:

$$\begin{cases} Y = \left[u \quad v \quad \frac{du}{dx} \quad \frac{dv}{dx} \quad \frac{d^2v}{dx^2} \quad \frac{d^3v}{dx^3} \right]^T \\ \frac{dY}{dx} = \left[\frac{du}{dx} \quad \frac{dv}{dx} \quad \frac{d^2u}{dx^2} \quad \frac{d^2v}{dx^2} \quad \frac{d^3v}{dx^3} \quad \frac{d^4v}{dx^4} \right]^T \\ u = [u_1 \quad \dots \quad u_P] \\ v = [v_1 \quad \dots \quad v_P] \end{cases} \quad (55)$$

In the frame of a 1D-beam kinematics, there are three degree of freedom (dof) per node. Therefore, one ME of P layers has a total of $6(P+1)$ dof. As a result, A is a square $6(P+1) \times 6(P+1)$ matrix, and Y is a column vector of size $6(P+1)$.

4.2 Particular cases

The SLJ is the particular case of $P = 2$. If $p = 0$ for Eq. (43) it leads to GR type. Supposing $H_i = H_i' = K_i = K_i' = 0$ with $1 \leq i \leq P$, the set of equations provided by Eqs. (44) – (52) is the same than Eq. (1) – (3). The DLJ (Fig. 4) is the particular case of $P = 3$. Assuming $p = 0$ for Eq. (43), the set of equations provided by Eqs. (44), (45), and (46) becomes:

$$\begin{cases} \frac{dN_1}{dx} + T_1 b = 0 \\ \frac{dV_1}{dx} - S_1 \cdot b = 0 \\ \frac{dM_1}{dx} + V_1 + T_1 b h_{1,1}^1 = 0 \end{cases} \quad (56)$$

$$\begin{cases} \frac{dN_2}{dx} - (T_1 - T_2) b = 0 \\ \frac{dV_2}{dx} + (S_1 - S_2) \cdot b = 0 \\ \frac{dM_2}{dx} + V_2 + (T_1 h_{2,1}^1 + T_2 h_{2,2}^1) b = 0 \end{cases} \quad (57)$$

$$\begin{cases} \frac{dN_3}{dx} - T_2 b = 0 \\ \frac{dV_3}{dx} + S_2 \cdot b = 0 \\ \frac{dM_3}{dx} + V_3 + T_2 b h_{3,2}^1 = 0 \end{cases} \quad (58)$$

Eq. (47) becomes:

$$\begin{cases} S_1 = k_{I,1} [v_1 - v_2] \\ T_1 = k_{II,1} [u_2 - u_1 - h_2 \theta_2 - h_1 \theta_1] \\ S_2 = k_{I,2} [v_2 - v_3] \\ T_2 = k_{II,2} [u_3 - u_2 - h_3 \theta_3 - h_2 \theta_2] \end{cases} \quad (59)$$

where:

$$\begin{cases} k_{I,1} = \frac{E_{a1}}{t_1} \\ k_{II,1} = \frac{G_{a1}}{t_1} \\ k_{I,2} = \frac{E_{a2}}{t_2} \\ k_{II,2} = \frac{G_{a2}}{t_2} \end{cases} \quad (60)$$

Assuming $H_i = H_i' = K_i = K_i' = 0$ with $1 \leq i \leq P$ and $B_i = 0$, the constitutive equations become, from Eqs.

(48), (49), and (50):

$$\begin{cases} N_1 = A_1 \frac{du_1}{dx} \\ M_1 = D_1 \frac{d\theta_1}{dx} \\ \theta_1 = \frac{dv_1}{dx} \end{cases} \quad (61)$$

$$\begin{cases} N_2 = A_2 \frac{du_2}{dx} \\ M_2 = D_2 \frac{d\theta_2}{dx} \\ \theta_2 = \frac{dv_2}{dx} \end{cases} \quad (62)$$

$$\begin{cases} N_3 = A_3 \frac{du_3}{dx} \\ M_3 = D_3 \frac{d\theta_3}{dx} \\ \theta_3 = \frac{dv_3}{dx} \end{cases} \quad (63)$$

Eq. (55) becomes:

$$\begin{cases} Y = \left[u \quad v \quad \frac{du}{dx} \quad \frac{dv}{dx} \quad \frac{d^2v}{dx^2} \quad \frac{d^3v}{dx^3} \right]^T \\ \frac{dY}{dx} = \left[\frac{du}{dx} \quad \frac{dv}{dx} \quad \frac{d^2u}{dx^2} \quad \frac{d^2v}{dx^2} \quad \frac{d^3v}{dx^3} \quad \frac{d^4v}{dx^4} \right]^T \\ u = [u_1 \quad u_2 \quad u_3] \\ v = [v_1 \quad v_2 \quad v_3] \end{cases} \quad (64)$$

After some simplification, Eq. (64) becomes:

$$\begin{cases} Y = \left[u_1 \quad u_2 \quad u_3 \quad v_1 \quad v_2 \quad v_3 \quad \frac{du_1}{dx} \quad \frac{du_2}{dx} \quad \frac{du_3}{dx} \quad \frac{dv_1}{dx} \quad \frac{dv_2}{dx} \quad \frac{dv_3}{dx} \quad \frac{d^2v_1}{dx^2} \quad \frac{d^2v_2}{dx^2} \quad \frac{d^2v_3}{dx^2} \quad \frac{d^3v_1}{dx^3} \quad \frac{d^3v_2}{dx^3} \quad \frac{d^3v_3}{dx^3} \right]^T \\ \frac{dY}{dx} = \left[\frac{du_1}{dx} \quad \frac{du_2}{dx} \quad \frac{du_3}{dx} \quad \frac{dv_1}{dx} \quad \frac{dv_2}{dx} \quad \frac{dv_3}{dx} \quad \frac{d^2u_1}{dx^2} \quad \frac{d^2u_2}{dx^2} \quad \frac{d^2u_3}{dx^2} \quad \frac{d^2v_1}{dx^2} \quad \frac{d^2v_2}{dx^2} \quad \frac{d^2v_3}{dx^2} \quad \frac{d^3v_1}{dx^3} \quad \frac{d^3v_2}{dx^3} \quad \frac{d^3v_3}{dx^3} \quad \frac{d^4v_1}{dx^4} \quad \frac{d^4v_2}{dx^4} \quad \frac{d^4v_3}{dx^4} \right]^T \end{cases} \quad (65)$$

Finally, Eq. (54) becomes:

$$\frac{dY}{dx} = A \cdot Y \quad (66)$$

with A , a square matrix provided in Appendix B. Thanks to the aforementioned, the general analytical solution of the system is determined where the characteristic polynomial is 18th order. It owns eight conjugate, four real and six null eigenvalues. Therefore, the nodal displacements and forces are determined. Then, the stiffness matrix K is computed. The free adherends are modeled as traditional Euler-Bernoulli laminated beam. For a symmetrical DLJ (Fig. 4), the properties used are listed in the Table 3. On one side, it is clamped and on the other side, loaded with a force $P = 100$ N.

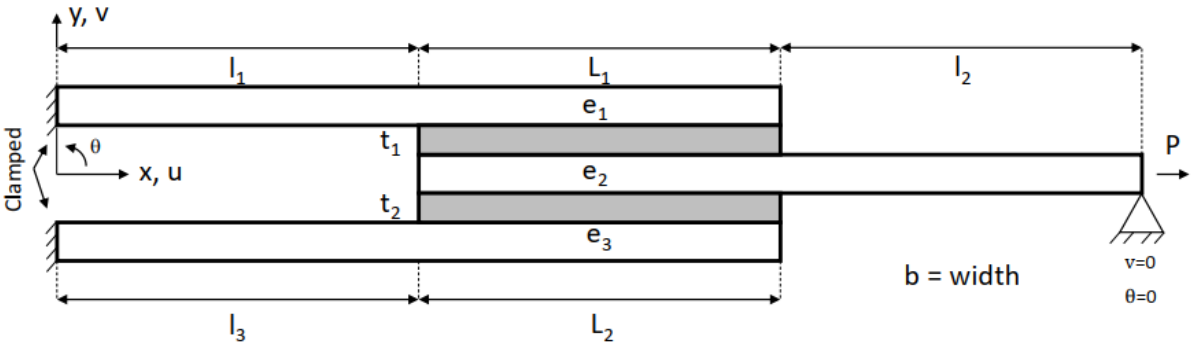


Figure 4. Double lap joint annotation.

Table 3. Double lap joint properties.

Adherend 1	$e_1 = 2$ mm	$b = 10$ mm	$l_1 = 100$ mm	$E_1 = 70$ GPa	$\nu_1 = 0.33$
Adhesive 1	$t_1 = 250$ μ m	$b = 10$ mm	$L_1 = 30$ mm	$E_{a1} = 2240$ MPa	$G_{a1} = 800$ MPa
Adherend 2	$e_2 = 2$ mm	$b = 10$ mm	$l_2 = 100$ mm	$E_2 = 70$ GPa	$\nu_2 = 0.33$
Adhesive 2	$t_2 = 250$ μ m	$b = 10$ mm	$L_2 = 30$ mm	$E_{a2} = 2240$ GPa	$G_{a2} = 800$ MPa
Adherend 3	$e_3 = 2$ mm	$b = 10$ mm	$l_3 = 100$ mm	$E_3 = 70$ GPa	$\nu_3 = 0.33$

A 1D FE models has been built with beam elements for the adherends and spring elements for the adhesive layer, to be as close as possible to the ME modelling hypothesis. The nodes associated with beam elements are located at the actual neutral line of adherends. The nodes associated with the spring elements are located at the actual interfaces of adherends. For each adherend along the overlap, rigid body elements were used to link the nodes of the neutral lines and to the nodes of the adherend interface. A scheme of the 1D FE model used is provided in Fig. 5. Beam elements are based

on degree 3 interpolating functions under the Euler-Bernoulli kinematics. The overlap length of adherends was then regularly meshed with the number of ME (n_{BE}). This parameter has been set to 600. The springs stiffnesses k_{ui} and k_{vi} are directly related to the mesh density along the overlap [51]. For a spring element located at an abscissa x along the overlap, the stiffnesses are computed from the value of adhesive peel and shear modulus, the adhesive thicknesses t_1 or t_2 , the width b and the mesh density $\frac{L}{n_{BE}}$ such as:

$$\begin{cases} k_{v1}(x) = m(x) \frac{L}{n_{BE}} b \frac{E_{a1}}{t_1} = m(x) \frac{L}{n_{BE}} b k_{I,1} \\ k_{u1}(x) = m(x) \frac{L}{n_{BE}} b \frac{G_{a1}}{t_1} = m(x) \frac{L}{n_{BE}} b k_{II,1} \\ k_{v2}(x) = m(x) \frac{L}{n_{BE}} b \frac{E_{a2}}{t_2} = m(x) \frac{L}{n_{BE}} b k_{I,2} \\ k_{u2}(x) = m(x) \frac{L}{n_{BE}} b \frac{G_{a2}}{t_2} = m(x) \frac{L}{n_{BE}} b k_{II,2} \end{cases} \quad (67)$$

where $m(x) = \begin{cases} \frac{1}{2} & \text{if } x = 0 \text{ or } L \\ 1 & \text{otherwise} \end{cases}$

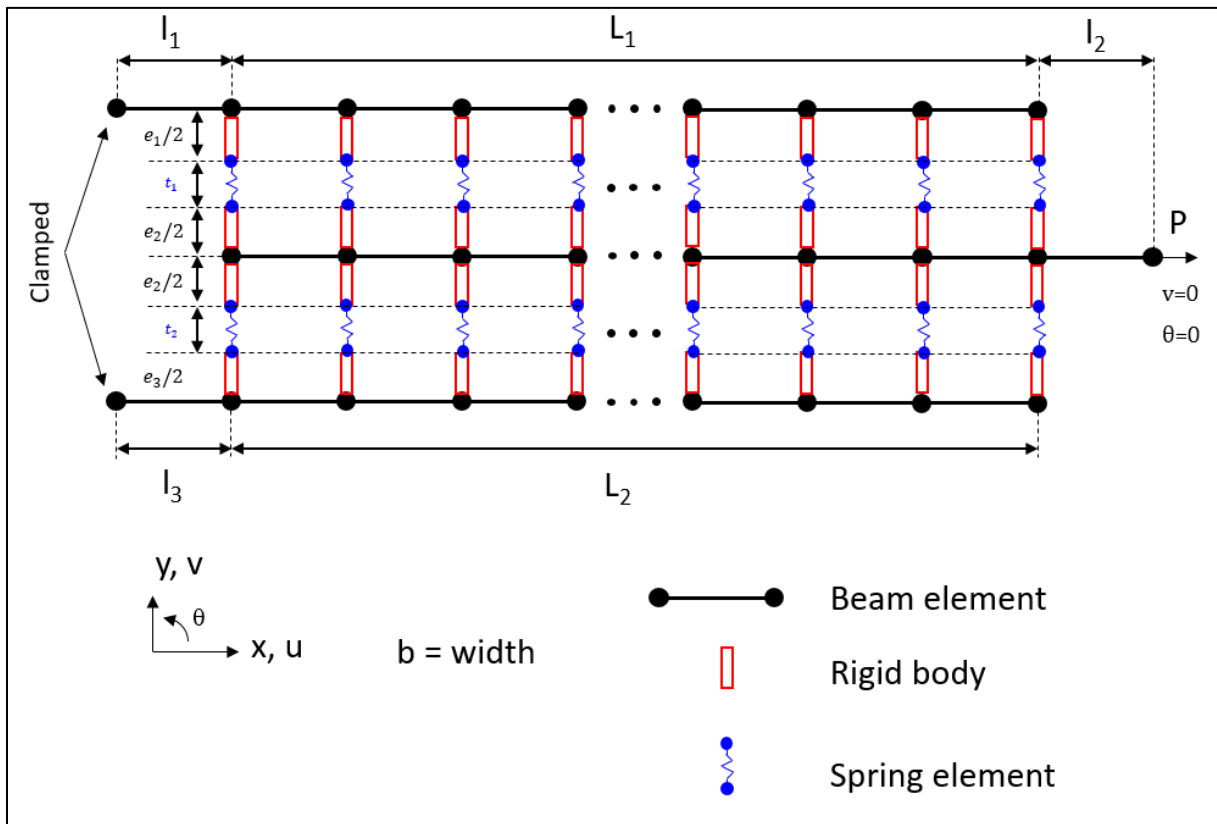


Figure 5. DLJ - Principle scheme for the 1D FE models.

The peel and shear stress distribution along the overlap of each adhesive layer are respectively represented on Fig. 6 and Fig. 7.

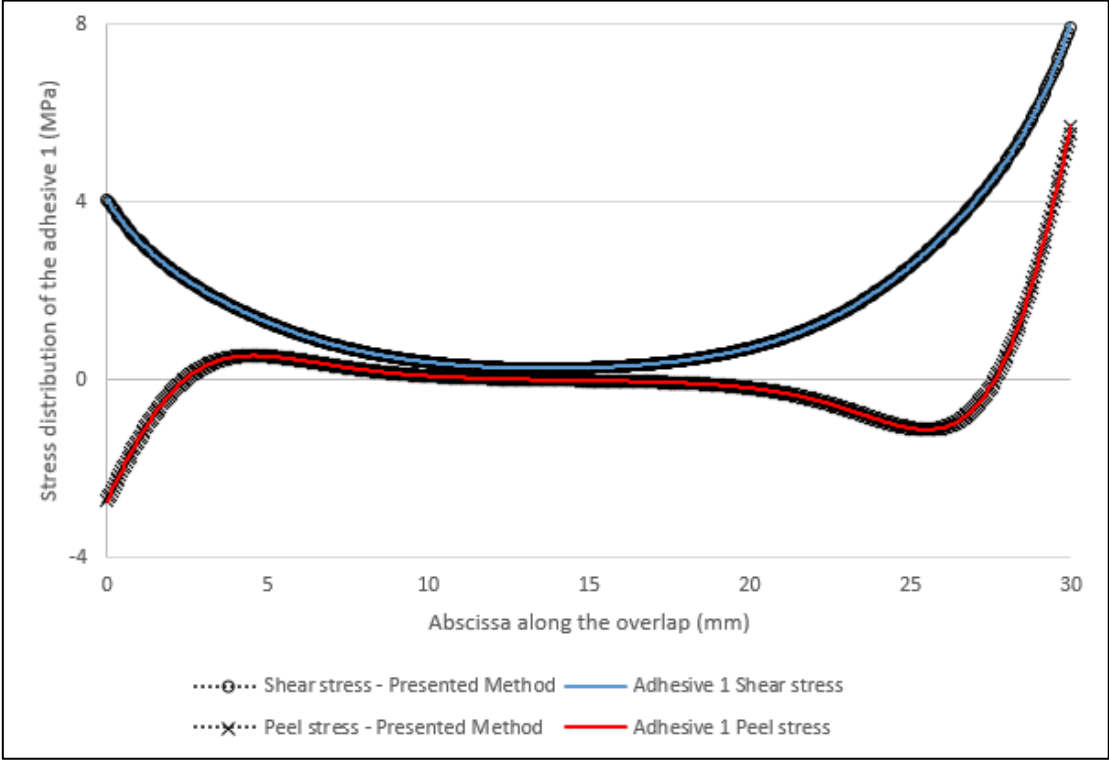


Figure 6. DLJ symmetric - Adhesive Peel and Shear stress along the overlap of the adhesive 1 with FE model.

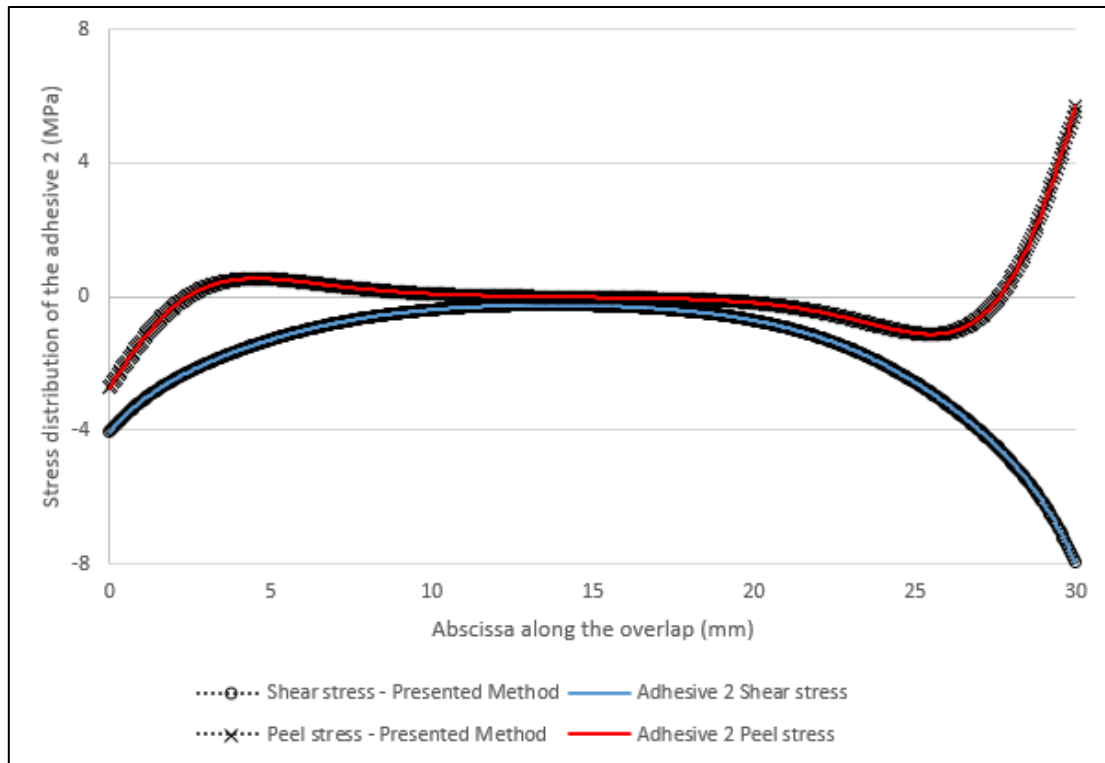


Figure 7. DLJ symmetric - Adhesive Peel and Shear stress along the overlap of the adhesive 2 with FE model.

As expected, the adhesive stresses are symmetrical with respect to the inner adherend. In magnitude, the stresses are equal, which are expected results. Fig. 6 and Fig. 7 presents good correlation. The presented method provide equivalent results than the 1D FE model. The maximum absolute error observed here is 0.1% along the overlap compared to the range of stress values. For a dissimilar DLJ (Fig. 4), the properties used are listed in the Table 4. Boundaries conditions are the same than previously. The peel and shear stress distribution along the overlap of each adhesive layer are respectively represented on Fig. 8 and Fig. 9.

Table 4. Dissimilar Double Lap Joint properties.

Adherend 1	$e_1 = 2 \text{ mm}$	$b = 10 \text{ mm}$	$l_1 = 100 \text{ mm}$	$E_1 = 70 \text{ GPa}$	$\nu_1 = 0.33$
Adhesive 1	$t_1 = 250 \text{ }\mu\text{m}$	$b = 10 \text{ mm}$	$L_1 = 30 \text{ mm}$	$E_{a1} = 2240 \text{ MPa}$	$G_{a1} = 800 \text{ MPa}$
Adherend 2	$e_2 = 2.5 \text{ mm}$	$b = 10 \text{ mm}$	$l_2 = 100 \text{ mm}$	$E_2 = 65 \text{ GPa}$	$\nu_2 = 0.33$

Adhesive 2	$t_2 = 150 \mu\text{m}$	$b = 10 \text{ mm}$	$L_2 = 30 \text{ mm}$	$E_{a2} = 1960 \text{ MPa}$	$G_{a2} = 700 \text{ MPa}$
Adherend 3	$e_3 = 1.5 \text{ mm}$	$b = 10 \text{ mm}$	$l_3 = 100 \text{ mm}$	$E_3 = 210 \text{ GPa}$	$\nu_3 = 0.33$

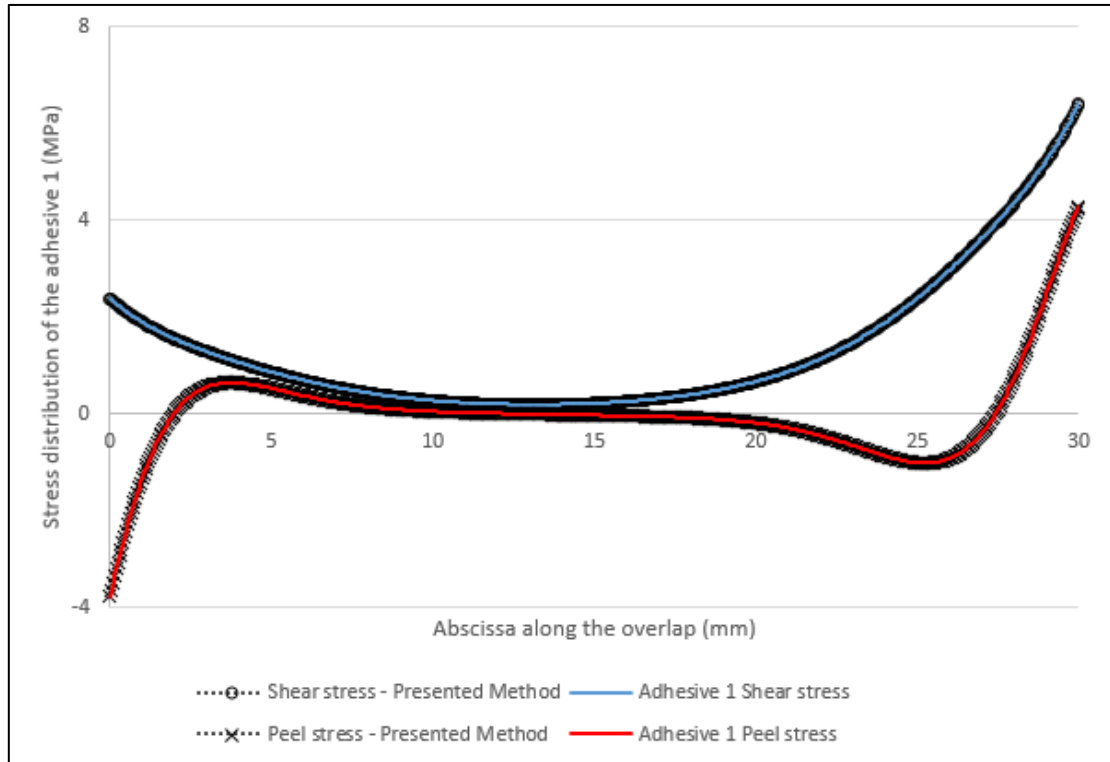


Figure 8. DLJ non-symmetric - Adhesive Peel and Shear relative stress error along the overlap of the adhesive 1 with FE model.

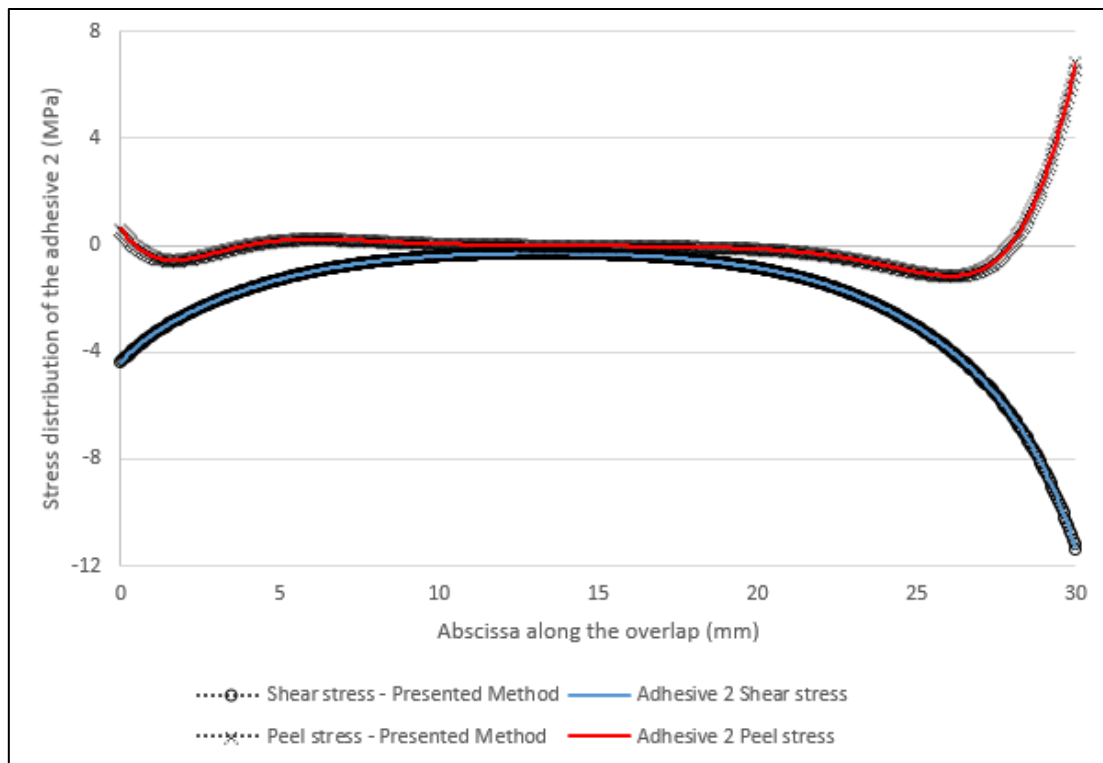


Figure 9. DLJ non-symmetric - Adhesive Peel and Shear stress along the overlap of the adhesive 2 with FE model.

As expected, the aforementioned method can deal with non-symmetrical geometry. The Fig. 8 and Fig. 9 presents good correlation. The presented method provide equivalent results than the 1D FE model. The maximum absolute error observed here is 0.1% along the overlap compared to the range of stress values.

5. Conclusion

Numerous models based on various sets of simplifying hypotheses exist to provide, at low computational time, accurate predictions of the mechanical behavior of bonded aircraft structures at the presizing stage. If closed-form solutions can sometimes be derived, the use of dedicated resolution schemes is mainly required to solve the system of ODEs coming from the simplifying hypotheses. The ME technique is one of these dedicated resolution schemes. It is based on the formulation the stiffness matrix of specific 4-nodes element to model a bonded overlap. The original methodology for the formulation of ME allows for the providing of the shape of solutions in terms of adherend

displacements and internal loads [24–28]. The direct consequence is that only one ME is needed to model the full length of the bonded overlap and then to obtain the distributions of adherend displacements and internal forces as well as the adhesive stresses at any abscissa of the overlap. However, it is difficult with the original method to take into account some variations in the set of simplifying hypotheses. A second methodology, making use of the exponential matrix, has then been suggested to quickly formulate the ME stiffness matrix when the simplifying hypotheses are modified [31, 32]. Nevertheless, the shape of solutions for the adherend displacements and internal force are not known anymore, so that the results are only available at nodes. It means that a dedicated mesh is required to post-process the result at any abscissa. In the present paper, a new methodology for the formulation of ME stiffness matrices is presented. This methodology offers the ability to easily take into account for the modification of simplifying hypotheses while providing the shape of solutions, which reduced then the computational time. The system of ODEs is solved using the Jordan form approach. This methodology is illustrated on the SLJ configuration step by step. The results provided are the same as those provided by the original approach by in terms of adhesive stresses. The methodology is then applied to formulate a multi-layered ME involving various local equilibrium equations and constitutive equations. This multi-layered ME is then illustrated on a DLJ configuration under a 1D-beam kinematics. In both illustrations, good results with 1D FE models have been obtained. The aforementioned method is a turnkey method for first order ODEs system with constant coefficients. On a different ODEs type, it has to be adapted. The use of Euler-Bernoulli beam model to model the adherends is not a restriction and other beam models, such as Timoshenko one, could be considered in the frame of this methodology. Finally, the presented research in this paper focus on the derivation of solution shapes of displacement field, in order to take benefit from the ME technique. The formulation methodology can be easily applied – and implemented in the computer code – from various sets of simplified hypotheses, chosen to describe at best the mechanical behavior of the bonded structure under consideration. This approach can be employed to model structural joining areas in-plane loaded or considered as mainly in-plane loaded, which exhibit complex geometries.

These areas can involve fasteners [30]. They can be subjected to a variation of temperature, making use of the equivalent nodal force approach available in the FE method [32]. Finally, nonlinear material behaviors can be supported by an analysis based on a dedicated iterative procedure as presented in [29, 30].

Acknowledgments

The author affiliated to Sogeti High Tech gratefully acknowledges the engineers and the managers involved in the development of JoSAT (Joint Stress Analysis Tool), which is an internal research program. The authors warmly acknowledge Mr Salah Seddiki² for the supplying of FE predictions.

Declarations of interest

None.

Appendixes.

A. Single Lap Joint

A1. Differential equation resolution

The system Eq. (8) leads to the following characteristic polynomial:

$$\begin{cases} P(R) = P_1(R) * P_2(R) \\ P_1(R) = R^3 \\ P_2(R) = R^3 + k_1R^2 + k_2R + k_3 \end{cases} \quad (68)$$

where:

$$\begin{cases} R = \lambda^2 \\ k_1 = -\frac{Gb}{e} \left(\frac{1}{A_1} + \frac{1}{A_2} + \frac{e_1^2}{4D_1} + \frac{e_2^2}{4D_2} \right) \\ k_2 = \frac{Eb}{e} \left(\frac{1}{D_1} + \frac{1}{D_2} \right) \\ k_3 = -\frac{EGb^2}{e^2} \left[\frac{1}{A_1D_1} + \frac{1}{A_2D_1} + \frac{1}{A_1D_2} + \frac{1}{A_2D_2} + \frac{(e_1+e_2)^2}{4D_1D_2} \right] \end{cases} \quad (69)$$

Looking for root square R of $P(R)$ in Eq. (68) is equivalent to the separated problem $P_1(R)$ and $P_2(R)$.

$P_1(R)$ and $P_2(R)$ have respectively 3 null (named R_4) and 3 non-null eigenvalues (named R_1, R_2, R_3).

Using the first relation from Eq. (69), R_i with $i \in [1,4]$ provides 6 null (named λ_7) and 6 non-null eigenvalues (named λ_i with $i \in [1,6]$). Cardan's method is used to determinate $P_2(R)$ eigenvalues of Eq. (68) by rewriting it as:

$$P_2(R') = R'^3 + \hat{p}R' + \hat{q} \quad (70)$$

where:

$$\begin{cases} R' = R - \frac{k_1}{3} \\ R = \lambda^2 \\ \hat{p} = -\frac{k_1^2}{3} + k_2 \\ \hat{q} = -\frac{k_1}{27}(2k_1^2 - 9k_2) + k_3 \\ \hat{\Delta} = 27\hat{q}^2 + 4\hat{p}^3 \end{cases} \quad (71)$$

According to the sign of the Cardan's discriminant, three specific cases can be distinguished: (i) $\Delta > 0$, (ii) $\Delta = 0$ and (iii) $\Delta < 0$. Each case leads to a set $\{R_1, R_2, R_3\}$ of eigenvalue of $P_2(R)$ and then to the set $\{\lambda_1, \lambda_2, \lambda_3, \lambda_4, \lambda_5, \lambda_6\}$ of eigenvalues of $P_2(\lambda)$. In a single lap joint (SLJ) problem, the most common case is the positive Cardan's discriminant [13]. The Cardan's discriminant solutions are:

$$\begin{cases} R'_1 = u + v = r^2 - \frac{k_1}{3} \\ R'_2 = j \cdot u + \bar{j} \cdot v = (s + i \cdot t)^2 - \frac{k_1}{3} \\ R'_3 = j^2 \cdot u + j \cdot v = (s - i \cdot t)^2 - \frac{k_1}{3} \end{cases} \quad (72)$$

where:

$$\begin{cases} u = \sqrt[3]{\frac{-\hat{q} + \sqrt{\hat{\Delta}/27}}{2}} \\ v = \sqrt[3]{\frac{-\hat{q} - \sqrt{\hat{\Delta}/27}}{2}} \\ j = j^2 = -\frac{1}{2} + i \frac{\sqrt{3}}{2} \\ j^2 = \bar{j} = -\frac{1}{2} - i \frac{\sqrt{3}}{2} \end{cases} \quad (73)$$

and where " i " refers to the imaginary unit so that $i^2 = -1$. Depending on the sign of the roots $\{R'_1, R'_2, R'_3\}$, the six roots $\{R_1, R_2, R_3, R_4, R_5, R_6\}$ of the characteristic polynomial can be defined using Eqs. (72) and (73) as:

$$R_1 = +r \quad R_2 = -r \quad R_3 = (s + it) \quad R_4 = (s - it) \quad R_5 = -(s + it) \quad R_6 = -(s - it) \quad (74)$$

Or:

$$R_1 = +ir \quad R_2 = -ir \quad R_3 = (s + it) \quad R_4 = (s - it) \quad R_5 = -(s + it) \quad R_6 = -(s - it) \quad (75)$$

depending on the sign of R'_1 in Eq. (72). Therefore, the adhesive shear and peel stress expressions are:

$$\begin{cases} S(x) = \left[\begin{array}{l} \bar{K}_1 e^{s.x} \sin(t.x) + \bar{K}_2 e^{s.x} \cos(t.x) + \bar{K}_3 e^{-s.x} \sin(t.x) \\ + \bar{K}_4 e^{-s.x} \cos(t.x) + \bar{K}_5 e^{r.x} + \bar{K}_6 e^{-r.x} \end{array} \right] \\ T(x) = \left[\begin{array}{l} K_1 e^{s.x} \sin(t.x) + K_2 e^{s.x} \cos(t.x) + K_3 e^{-s.x} \sin(t.x) \\ + K_4 e^{-s.x} \cos(t.x) + K_5 e^{r.x} + K_6 e^{-r.x} + K_7 \end{array} \right] \end{cases} \quad (76)$$

where \bar{K}_j with $j \in [1,6]$ and K_j with $j \in [1,7]$ are integration constants, which can be expressed as combinations of c_i with $i \in [1,12]$ from Eq. (9). By combining Eqs. (1), (5), and (76), the nodal displacements and forces are expressed to compute Eq. (10) which provides the stiffness matrix with Eq. (11).

A2. Matrix representation

The square matrix A used in Eq. (15) is the following:

$$A = \begin{bmatrix} 0 & 0 & 0 & 0 & 1 & 0 & 0 & 0 & 0 & 0 & 0 & 0 \\ 0 & 0 & 0 & 0 & 0 & 1 & 0 & 0 & 0 & 0 & 0 & 0 \\ 0 & 0 & 0 & 0 & 0 & 0 & 1 & 0 & 0 & 0 & 0 & 0 \\ 0 & 0 & 0 & 0 & 0 & 0 & 0 & 1 & 0 & 0 & 0 & 0 \\ a_{5,1} & a_{5,2} & 0 & 0 & 0 & 0 & a_{5,7} & a_{5,8} & 0 & 0 & 0 & 0 \\ a_{6,1} & a_{6,2} & 0 & 0 & 0 & 0 & a_{6,7} & a_{6,8} & 0 & 0 & 0 & 0 \\ 0 & 0 & 0 & 0 & 0 & 0 & 0 & 0 & 1 & 0 & 0 & 0 \\ 0 & 0 & 0 & 0 & 0 & 0 & 0 & 0 & 0 & 1 & 0 & 0 \\ 0 & 0 & 0 & 0 & 0 & 0 & 0 & 0 & 0 & 0 & 1 & 0 \\ 0 & 0 & 0 & 0 & 0 & 0 & 0 & 0 & 0 & 0 & 0 & 1 \\ 0 & 0 & a_{11,3} & a_{11,4} & a_{11,5} & a_{11,6} & 0 & 0 & a_{11,9} & a_{11,10} & 0 & 0 \\ 0 & 0 & a_{12,3} & a_{12,4} & a_{12,5} & a_{12,6} & 0 & 0 & a_{12,9} & a_{12,10} & 0 & 0 \end{bmatrix} \quad (77)$$

The components of the matrix A in Eq. (25) are given in Table A-1.

Table A-1. Constant expression of Eq. (77)

$a_{5,1} = \frac{Gb}{eA_1}$	$a_{5,7} = \frac{Gbe_1}{2eA_1}$	$a_{6,1} = -\frac{Gb}{eA_2}$	$a_{6,7} = -\frac{Gbe_1}{2eA_2}$
$a_{5,2} = -\frac{Gb}{eA_1}$	$a_{5,8} = \frac{Gbe_2}{2eA_1}$	$a_{6,2} = \frac{Gb}{eA_2}$	$a_{6,8} = -\frac{Gbe_2}{2eA_2}$
$a_{11,3} = -\frac{Eb}{eD_1}$	$a_{11,5} = \frac{Gbe_1}{2eD_1}$	$a_{11,9} = \frac{Gbe_1^2}{4eD_1}$	

$a_{11,4} = \frac{Eb}{eD_1}$	$a_{11,6} = -\frac{Gbe_1}{2eD_1}$	$a_{11,10} = \frac{Gbe_1e_2}{4eD_1}$	
$a_{12,3} = \frac{Eb}{eD_2}$	$a_{11,5} = \frac{Gbe_2}{2eD_2}$	$a_{11,9} = \frac{Gbe_1e_2}{4eD_2}$	
$a_{12,4} = -\frac{Eb}{eD_2}$	$a_{11,6} = -\frac{Gbe_2}{2eD_2}$	$a_{11,10} = \frac{Gbe_2^2}{4eD_2}$	

B. Double lap joint matrix coefficients

By combining Eqs. (56), (59), (61), and (62), it comes:

$$\frac{d^2u_1}{dx^2} = \left(\frac{bG_{a1}}{A_1t_1}\right)u_1 + \left(-\frac{bG_{a1}}{A_1t_1}\right)u_2 + \left(\frac{bG_{a1}e_1}{2A_1t_1}\right)\frac{dw_1}{dx} + \left(\frac{bG_{a1}e_2}{2A_1t_1}\right)\frac{dw_2}{dx}$$

$$\frac{d^4w_1}{dx^4} = \left(\frac{be_1G_{a1}}{2t_1D_1}\right)\frac{du_1}{dx} + \left(-\frac{be_1G_{a1}}{2t_1D_1}\right)\frac{du_2}{dx} + \left(-\frac{bE_{a1}}{t_1D_1}\right)w_1 + \left(\frac{bE_{a1}}{t_1D_1}\right)w_2 + \left(\frac{be_1^2G_{a1}}{4t_1D_1}\right)\frac{d^2w_1}{dx^2} + \left(\frac{be_1e_2G_{a1}}{4t_1D_1}\right)\frac{d^2w_2}{dx^2}$$

such as:

$$\frac{d^2u_1}{dx^2} = k_1u_1 + k_2u_2 + k_3\frac{dw_1}{dx} + k_4\frac{dw_2}{dx}$$

$$\frac{d^4w_1}{dx^4} = k_{15}\frac{du_1}{dx} + k_{16}\frac{du_2}{dx} + k_{17}w_1 + k_{18}w_2 + k_{19}\frac{d^2w_1}{dx^2} + k_{20}\frac{d^2w_2}{dx^2}$$

By combining Eqs. (57), (59), (61), (62), and (63), it comes:

$$\frac{d^2u_2}{dx^2} = \left(-\frac{bG_{a1}}{A_2t_1}\right)u_1 + \left(\frac{bG_{a1}}{A_2t_1} + \frac{bG_{a2}}{A_2t_2}\right)u_2 + \left(-\frac{bG_{a2}}{A_2t_2}\right)u_3 + \left(-\frac{bG_{a1}e_1}{2A_2t_1}\right)\frac{dw_1}{dx} + \left(-\frac{bG_{a1}e_2}{2A_2t_1} + \frac{bG_{a2}e_2}{2A_2t_2}\right)\frac{dw_2}{dx} +$$

$$\left(\frac{bG_{a2}e_3}{2A_2t_2}\right)\frac{dw_3}{dx}$$

$$\frac{d^4w_2}{dx^4} = \left(\frac{be_2G_{a1}}{2t_1D_2}\right)\frac{du_1}{dx} + \left(\frac{be_2G_{a2}}{2t_2D_2} - \frac{be_2G_{a1}}{2t_1D_2}\right)\frac{du_2}{dx} + \left(-\frac{be_2G_{a2}}{2t_2D_2}\right)\frac{du_3}{dx} + \left(\frac{bE_{a1}}{t_1D_2}\right)w_1 + \left(-\frac{bE_{a1}}{t_1D_2} - \frac{bE_{a2}}{t_2D_2}\right)w_2 +$$

$$\left(\frac{bE_{a2}}{t_2D_2}\right)w_3 + \left(\frac{be_1e_2G_{a1}}{4t_1D_2}\right)\frac{d^2w_1}{dx^2} + \left(\frac{be_2^2G_{a1}}{4t_1D_2} + \frac{be_2^2G_{a2}}{4t_2D_2}\right)\frac{d^2w_2}{dx^2} + \left(\frac{be_2e_3G_{a2}}{4t_2D_2}\right)\frac{d^2w_3}{dx^2}$$

such as:

$$\frac{d^2u_2}{dx^2} = k_5u_1 + k_6u_2 + k_7u_3 + k_8\frac{dw_1}{dx} + k_9\frac{dw_2}{dx} + k_{10}\frac{dw_3}{dx}$$

$$\frac{d^4w_2}{dx^4} = k_{21}\frac{du_1}{dx} + k_{22}\frac{du_2}{dx} + k_{23}\frac{du_3}{dx} + k_{24}w_1 + k_{25}w_2 + k_{26}w_3 + k_{27}\frac{d^2w_1}{dx^2} + k_{28}\frac{d^2w_2}{dx^2} + k_{29}\frac{d^2w_3}{dx^2}$$

By combining Eqs. (58), (59), (63), and (64), it comes:

$$\frac{d^2u_3}{dx^2} = \left(-\frac{bG_{a2}}{A_3t_2}\right)u_2 + \left(\frac{bG_{a2}}{A_3t_2}\right)u_3 + \left(-\frac{bG_{a2}e_2}{2A_3t_2}\right)\frac{dw_2}{dx} + \left(-\frac{bG_{a2}e_3}{2A_3t_2}\right)\frac{dw_3}{dx}$$

- [14] Bigwood, D. A., and Crocombe, A. D. *Int. J. Adhes. Adhes.* 9 (4), 229–242 (1989). DOI: 10.1016/0143-7496(89)90066-3.
- [15] Oplinger, D. W. US AMTL Technical Report MTL91-23, (1991).
- [16] Tsai, M. Y., Oplinger, D. W., and Morton, J. *Int. J. Solids Struct.* 35 (12), 1163–1185 (1998). DOI: 10.1016/S0020-7683(97)00097-8.
- [17] Högberg, L. Mechanical Behaviour of Single-Layer Adhesive Joints : An Integrated Approach. Licensing Graduate Thesis, Chalmers University of Technology: Sweden, 2004.
- [18] Nemes, O., and Lachaud, F. *J. Adhes. Sci. Technol.* 23 (10–11), 1383–1393 (2009). DOI: 10.1163/156856109X432983.
- [19] Luo, Q., and Tong, L. *Int. J. Adhes. Adhes.* 29 (2), 144–154 (2009). DOI: 10.1016/j.ijadhadh.2008.01.007.
- [20] Weißgraeber, P., Stein, N., and Becker, W. *Int. J. Adhes. Adhes.* 55, 56–63 (2014). DOI: 10.1016/j.ijadhadh.2014.06.009.
- [21] Mortensen, F., and Thomsen, O. T. *Compos. Struct.* 38 (1), 281–294 (1997). DOI: 10.1016/S0263-8223(97)00063-9.
- [22] Mortensen, M. Development of Tools for Engineering Analysis and Design of High-Performance FRP-Composite Structural Elements. PhD Thesis, Aalborg University: Denmark, 1998.
- [23] Mortensen, F., and Thomsen, O. T. *Compos. Sci. Technol.* 62 (7–8), 1011–1031 (2002). DOI: 10.1016/S0266-3538(02)00030-1.
- [24] Paroissien, E. Contribution aux Assemblages Hybrides (Boulonnés/Collés) – Application aux Jonctions Aéronautiques. PhD Dissertation (in French), Université de Toulouse III: Toulouse, 2006.
- [25] Paroissien, E., Sartor, M., and Huet, J. Hybrid (Bolted/Bonded) Joints Applied to Aeronautic Parts: Analytical One-Dimensional Models of a Single-Lap Joint. In *Advances in Integrated Design and Manufacturing in Mechanical Engineering II*, Tichkiewitch, S., Tollenaere, M., Ray, P., Eds., Springer Netherlands: Dordrecht, pp 95–110, (2007). DOI: 10.1007/978-1-4020-6761-7_7.
- [26] Paroissien, E., Sartor, M., Huet, J., and Lachaud, F. *J. Aircr.* 44 (2), 573–582 (2007). DOI: 10.2514/1.24452.
- [27] Paroissien, E., Lachaud, F., and Jacobs, T. A Simplified Stress Analysis of Bonded Joints Using Macro-Elements. In *Advances in Modeling and Design of Adhesively Bonded Systems*, Kumar, S., Mittal, K. L., Eds., John Wiley & Sons, Inc.: Hoboken, NJ, USA, pp 93–146, (2013). DOI: 10.1002/9781118753682.ch4.
- [28] Paroissien, E., Gaubert, F., Da Veiga, A., and Lachaud, F. *J. Adhes. Sci. Technol.* 27 (13), 1464–1498 (2013). DOI: 10.1080/01694243.2012.745053.
- [29] Lelias, G., Paroissien, E., Lachaud, F., Morlier, J., Schwartz, S., and Gavaille, C. *Int. J. Solids Struct.* 62, 18–38 (2015). DOI: 10.1016/j.ijsolstr.2014.12.027.
- [30] Paroissien, E., Lachaud, F., Schwartz, S., Da Veiga, A., and Barrière, P. *Int. J. Adhes. Adhes.* 77, 183–197 (2017). DOI: 10.1016/j.ijadhadh.2017.05.003.
- [31] Paroissien, E., Lachaud, F., Morlier, J., and Schwartz, S. *Rev. Adhes. Adhes.* (2018). DOI: 10.7569/RAA.2018.097301.
- [32] Paroissien, E., da Silva, L. F. M., and Lachaud, F. *Compos. Struct.* 203, 85–100 (2018). DOI: 10.1016/j.compstruct.2018.07.015.
- [33] Jones, R. M. Composite materials, Mechanical behavior and structural analysis. Springer: New York, (1999).
- [34] Berthelot, J.-M. Composite materials, Mechanical behavior and structural analysis. Springer: New York, 1999.
- [35] Brualdi, R. A. *Am. Math. Mon.* 94 (3), 257 (1987). DOI: 10.2307/2323392.

- [36] Cater, S. *Am. Math. Mon.* 69 (5), 391 (1962). DOI: 10.2307/2312130.
- [37] Fletcher, R., and Sorensen, D. C. *Am. Math. Mon.* 90 (1), 12 (1983). DOI: 10.2307/2975686.
- [38] Galperin, A., and Waksman, Z. *Am. Math. Mon.* 87 (9), 728 (1980). DOI: 10.2307/2321861.
- [39] Gohberg, I., and Goldberg, S. *Am. Math. Mon.* 103 (2), 157 (1996). DOI: 10.2307/2975110.
- [40] Valiaho, H. *Am. Math. Mon.* 93 (9), 711 (1986). DOI: 10.2307/2322285.
- [41] Beauregard, R. A. Fraleigh, J. B. *A First Course in Linear Algebra with Optional Introduction to Groups, Rings, and Fields.* Boston: Houghton Mifflin (1973)
- [42] Golub, G. H. Van Loan, C. F. *Matrix Computation*, 3rd edition. The John Hopkins University Press, Baltimore, Maryland 1996.
- [43] Nering, E. D. *Linear Algebra and Matrix Theory*, 2nd edition, John Wiley and Sons: New-York, (1970).
- [44] Brechenmacher, F. *Histoire du théorème de Jordan de la décomposition matricielle (1870-1930). Formes de représentation et méthodes de décomposition.* PhD Thesis, Ecole des Hautes Etudes en Sciences Sociales (EHESS): France, 2006.
- [45] Horn, R. A. Johnson, C. R. *Matrix Analysis*, Cambridge University Press: New York 1985.
- [46] Gauthier-Villars., J. C.; *Traité des substitutions et des équations algébriques:* Paris, France (1870).
- [47] C. Jordan, *OEuvres de Camille Jordan*, Gauthier-Villars: Paris, 1961.
- [48] R. Bronson, *Matrix Methods: An Introduction.* Academic Press: New York, 1970.
- [49] Lélias, G., Paroissien, E., Lachaud, F., and Morlier, J. *Int. J. Solids Struct.* 158, 90–115 (2019). DOI: 10.1016/j.ijstr.2018.09.005.
- [50] Paroissien, E., Lachaud, F., da Silva, L. F. M., and Seddiki, S. *Compos. Struct.* 215, 331–350 (2019). DOI: 10.1016/j.compstruct.2019.02.070.
- [51] Dechwayukul, C., Rubin, C. A., and Hahn, G. T. *AIAA J.* 41 (11), 2216–2228 (2003). DOI: 10.2514/2.6814.